SAFER OPERATIONAL CONDITIONS FOR NATURAL GAS PROCESSING IN TRANSMISSION LINE TO LNG PLANTS

A Thesis

by

WONGWARAN ANDREW NAPAPORN

Submitted to the Office of Graduate and Professional Studies of
Texas A&M University
in partial fulfillment of the requirements for the degree of

MASTER OF SCIENCE

Chair of Committee,	Mahmoud El-Halwagi
Committee Members,	Farzan Sasangohar
	Ahmad Hilaly
Head of Department,	M. Nazmul Karim

December 2018

Major Subject: Chemical Engineering

Copyright 2018 Wongwaran Andrew Napaporn

ABSTRACT

Carbon dioxide must be removed from natural gas before liquefying the gas because it freezes in pipelines and corrodes process equipment. There are several processes that can be used to remove CO_2 from natural gas. The most common processes are chemical and physical absorption. Implementation of other processes such as adsorption, membrane separations and cryogenic distillations are also found all over the world. However, only chemical absorption and physical absorption processes meet the specification of CO_2 to be less than the required specification in the United States for preventing corrosion in transmission lines. Therefore, the current study focuses on these two processes. In each process, there are various ways to operate. The objective of this work is to find the optimal process and operating conditions, which cost us the least between the two given where the specification of the natural gas is achieved. Aspen HYSYS was used to simulate all the processes mentioned and Aspen Economic Evaluation was used to calculate the expenses of the processes. Corrosion rate and pipeline cost were evaluated using the NORSOK corrosion model. The process operational cost and pipeline cost have been evaluated and compared to find the suitable CO_2 removal process and optimal condition for various pipeline distance.

ACKNOWLEDGEMENTS

I would like to thank my dear advisor and was my committee chair, Dr. Sam Mannan who sadly passed away in September 2018. I am really honored to be advised by a man of his knowledge. This work cannot be done without his help. I would also like to thank Dr. Mahmoud El-Halwagi who was once my committee member and stepped up and take the role of my chair in place of Dr. Mannan for all the guidance and support throughout the course of my research. I am grateful and would like to also thank you Dr. Farzan Sasangohar and Dr. Ahmad Hilaly who are my committee members for all other advises which are very useful for my project.

I thank my team leader, Dr. Noor Quddus for aiding me in every way from commenting on my presentations to helping me getting the research done throughout my time here. I would like to also thank Dr. Harendra Mondal who helped me with the simulations and project calculations.

I also thank my friends at Mary Kay O'Connor Process Safety Center, the department faculty and staff for the experiences here at Texas A&M University that I will not forget for the rest of my days.

I would also want to mention all my dear Thai fellows, both seniors and juniors here at Texas A&M University for staying beside me and cheering me up when I was having a rough time throughout the period of my work.

Lastly, I would like to thank you my parents and brother, for their encouragement during my hardest time, their patience and most importantly, love.

CONTRIBUTORS AND FUNDING SOURCES

The project is supervised by Dr. M. Sam Mannan, my advisor, Dr. Mahmoud El-Halwagi, Dr. Ahmad Hilaly and Dr. Farzan Sasangohar, my chair and committee members. Financial support for the research was provided by Dr. M. Sam Mannan and all work in this thesis was done independently by the student.

TABLE OF CONTENTS

LIST OF FIGURES

Page

LIST OF TABLES

Page

CHAPTER I

INTRODUCTION

Liquefied Natural Gas (LNG) had a global trade of 244.8 tons in 2015 and tends to increase every year due to the new importers from Europe and the Middle East. In the US, several liquefaction projects are also targeting Final Investment Decisions (FID) in 2016. Targeting on 92.5 MTPA of capacity in total [1, 2]. LNG production can be expressed in simple steps as shown in Figure 1.

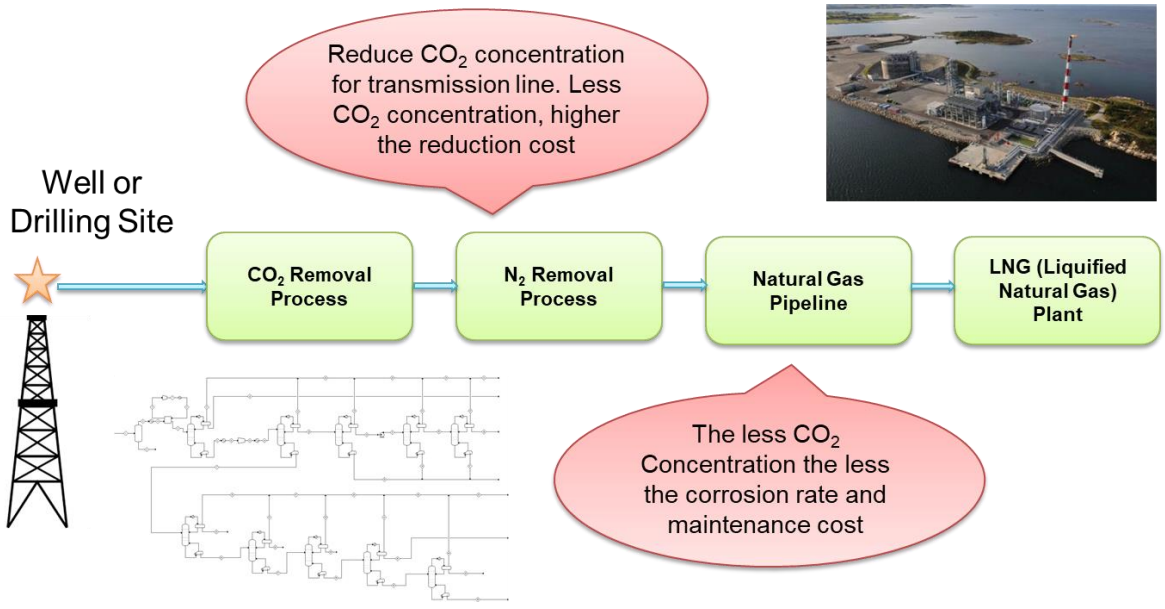

Figure 1: LNG Production Overview

As shown in the Figure 1, before natural gas can go through the liquefaction process to produce LNG, acid gas and other contamination must be removed. Carbon dioxide (CO_2) is one of the acid gases that is needed to be removed. CO_2 can be very dangerous if left in the natural gas.

Liquefaction process operates at a very low temperature and pressure, will freeze out any remaining CO_2 on exchanger surfaces, plugging pipelines and eventually harm the plant efficiency. Therefore, to prevent corrosion and freezing inside the process equipment and also to reach the LNG product specifications, removal of CO_2 is required [3].

The objective of this work is, to find the suitable commercialized process that can reduced the amount of CO_2 to the satisfied specification. Second objective is to determine the cost of the processes chosen and the cost from the CO_2 corrosion. The final goal is to compare the processes by using an economic factor to find the most appropriate process for a certain natural gas concentration and pipeline length.

1.1 CO_2 Removal Processes

Carbon capture technologies in natural gas are usually known as gas sweetening process such as: chemical absorption, physical absorption, membrane separation, low-temperature distillation and other approaches.

1.1.1 Chemical Absorption

There are many substances that can be used to remove CO_2 by chemical absorption process. For example, mono ethanolamine (MEA), methyl diethanolamine (MDEA), diglycolamine (DGA), diisopropanolamine (DIPA). These amines will react with CO_2 to form carbonate and bicarbonate to then be stripped, recycled and used again in the process [3]. Apart from amines, ammonia also offers the probability for developing absorption based on its less corrosiveness and its stability. In addition, carbonate based substances are also an option for chemical absorption processes [4, 5]. The chemical absorption process using amine is exhibited in Figure 2.

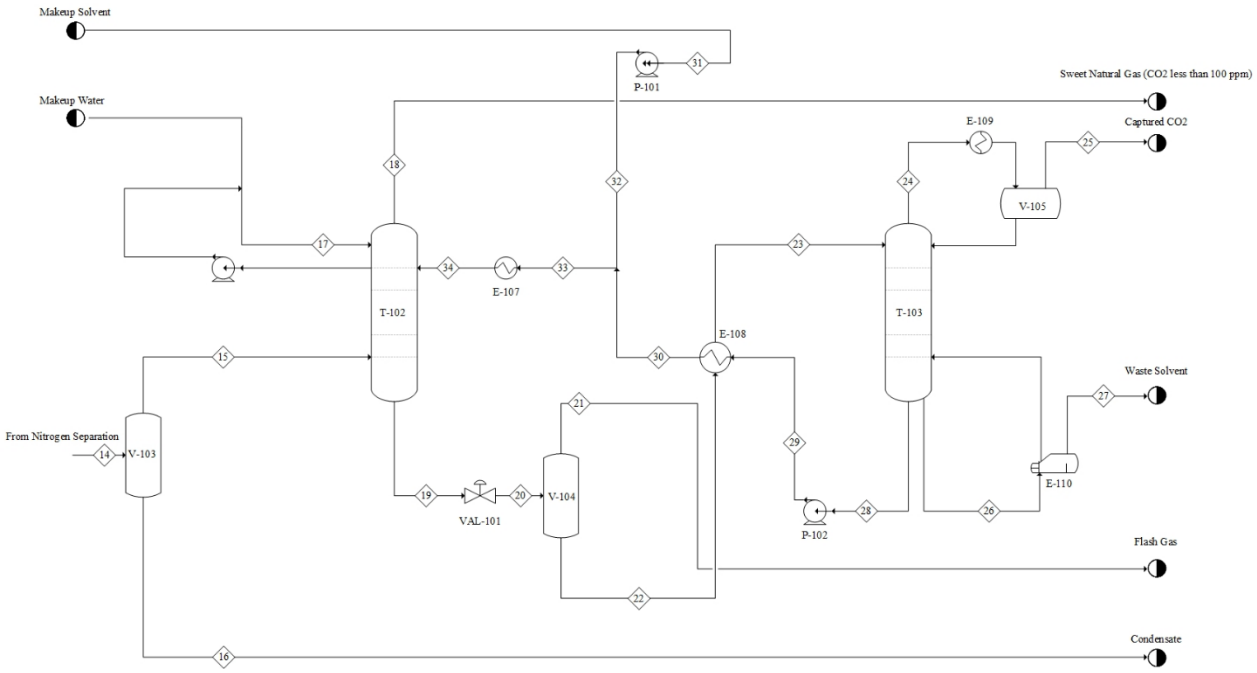

Figure 2: CO_2 Removal by amine absorpton process [6]

As shown in Figure 2, natural gas is fed into a separator, then CO_2 is removed by the amine in an absorber. Sweet gas is sent for further treatment and the rich amine solvent is recycled. The reaction occuring inside the absorber is as follow.

$$RNH_2 + CO_2 + H_2O \leftrightarrow (RNH_3)CO_3 \quad (1)$$

$$(RNH_3)CO_3 + CO_2 + H_2O \leftrightarrow 2RNH_3HCO_3 \quad (2)$$

Where R is the amine group [7]. The amine group is different according to the amine chosen. The following table shows the capacity of each amine in industries.

Table 1: Amines Relative Capacities [8]

Amine Type	Relative Acid Gas Capacity (%)	Remarks
Ethanolamine/Monoethanolamine	100	Difficult for H_2S
Diethanolamine	58	Reacts slowly
Triethanolamine	41	Low reactivity for H_2S
Diglycolamine	58	Similar to MEA
Diisopropanolamine	46	Selectivity of H_2S over CO_2
Methyldiethanolamine	51	Selectivity of H_2S over CO_2

However, even if the capacities of some of the amines or the selectivity of them do not lean towards CO_2, the result from using the any amine are similar when dealing with CO_2 removing. Therefore, using any type of amine would give similar results to the other amines.

Inorganic substances can also be used to capture CO_2. For example, potassium carbonate or sodium carbonate which the reactions are as follow [7].

$$Na_2CO_3 + CO_2 + H_2 \leftrightarrow 2NaHCO_3 \quad (3)$$

$$K_2CO_3 + CO_2 + H_2 \leftrightarrow 2KHCO_3 \quad (4)$$

Comparing between amine and inorganic chemical absorption requires the amine process is insensitive to operating pressure while the inorganic process has its pressure higher than 10337.76 mmHg. The operating temperature for amine process is between 37.78 – 204.44 C while inorganic is 93.33 – 121.11 C. Focusing on utility cost, the amine process is consider higher than the inorganic process [9].

To summarize the chemical absorption process limitations and challenges, mine solvent can cause corrosion of the process units and can eventually cause erosion to the equipment.

Moreover, since all the solvents used in the adsorption process cannot be completely recycled back to the process, disposal becomes an added concern. It can also cause environmental hazards as well as process hazards [7].

1.1.2 Physical Absorption

Physical absorption is a process which the solvent does not react with the dissolved gas. It only interacts with the gas physically. Capturing CO_2 from the feed gas is based on the solubility of CO_2 within the solvents. The two major factors that is used to determine the solubility of CO_2 are the feed gases' partial pressure and temperature. However, not all the processes available now are capable of meeting the specification of 50 – 100 ppmv of < 2.5% of CO_2 in the product gas stream [7]. A physical solvent that is commonly used is selexol, a liquid glycol-based solvent. It has been used for decades in natural gas processing. Glycol is considered to be very effective in removing CO_2 but it is captured near atmospheric pressure requiring recompression for transportation and storage [10]. The process using physical solvent can be roughly shown in Figure 3.

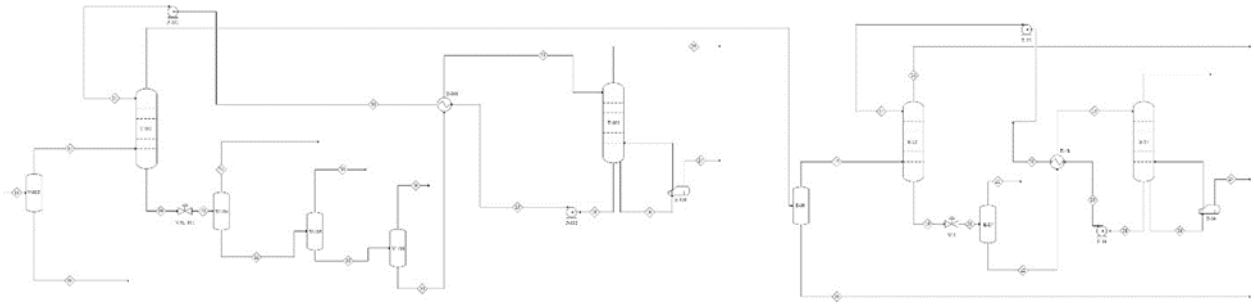

Figure 3: CO_2 removal by physical absorption

From *Figure 3* that, the physical absorption process is similar to chemical absorption but no reaction occurs in the absorber. The process operating pressure is between 17 – 68 bar, the operating temperature is at ambient temperature and the operating cost is relatively low comparing to chemical absorption [9].

1.1.3 Adsorption

Adsorption process uses solid adsorbent to adsorb the acid gas components from the flue gas. The process can occur either by ionic bonding of solids particles with the sour gas or chemical reaction (chemisorption). Iron oxide, Zinc oxide and molecular sieve (Zeolite) process are commonly used [3]. For chemisorption, it is considered as the formation of chemical bond between the sorbate and the solid surface. However, chemisorption suffers the difficulty of regenerating which can make it unsuitable for most process applications [11]. Therefore, physical surface adsorption is more applicable to most process nowadays. There are two main types of adsorption: thermal swing adsorption and pressure swing adsorption.

1.1.3.1 Thermal Swing Adsorption (TSA)

Thermal swing adsorption (TSA) is widely used for CO_2 removal. It is very reliable to remove minor components. Thermal adsorption is carried out by increasing the temperature of the adsorption bed by putting heat to it or purging it with high temperature purge gas. Nevertheless, there are some limitations for TSA. The cycle time that is required to cool down the bed is one of the issues. Moreover, high energy requirement and massive amount of heat loss is also another problem for this process to be consider (more than 30 kJ/mol) [7].

1.1.3.2 Pressure Swing Adsorption (PSA)

Pressure swing adsorption (PSA) is known as one of the most common process for gas separation in industries. PSA is a very well known method for the removal of CO_2 from natural

gas. The concept of PSA is by lowering the operational partial pressure to desorb the adsorbate. This can be carried out by depressurization or evacuation or both. In most adsorption process, each bed undergoes adsorption and regeneration cycle steps. Firstly, pressurization occurs followed by high pressure feed and co-current depressurization. After that, it goes through a countercurrent depressurization and a counter current purge. Finally, several equalizations between two beds are done [7].

Table 2 shows the typical loading capacities of some commercial adsorbents for acid gas removal with their suitable methods.

Table 2: Common CO2 loading capacities for adsorbents at certain operating conditions [8]

Adsorbent	**Adsorbate**	**Pressure (mmHg)**	**Temperature (C)**	**Regeneration Method**
Activated Carbon	CO_2	500	25-300	PSA
5A Zeolite	CO_2	500	25-250	PSA
Titanoilicates	CO_2	760×10^5	25-200	PSA
HTlc	CO_2	200-700	300-400	PSA
Solid amine	CO_2	760	75	PSA
Double-layered hydroxide	CO_2	230	375	PSA
Alumina (un-doped)	CO_2	500	400	PSA

Table 2 Continued

Adsorbent	**Adsorbate**	**Pressure (mmHg)**	**Temperature (C)**	**Regeneration Method**
Alumina (doped)	CO_2	500	400	PSA
Alumina (basic)	CO_2	500	300	PSA
Li zirconte	CO_2	760	500	TSA
CaO	CO_2	150	500	TSA

For adsorption, both TSA and PSA have their own benefits and drawbacks. The advantages of TSA is it is a process that is good for strongly adsorbed species, because small change in temperature gives large change in adsorbate and it is applicable for both gases and liquid. However, the heat loss is very high, and it is unsuitable for rapid cycling. Thus, adsorbent cannot be used with maximum efficacy. Also, in liquid systems, high latent heat of interstitial liquid must be added. For PSA, it is good where weakly adsorbed species is required in high purity. The process can use the adsorbent efficiently. Another drawback is its potentially low pressure requirement which is more expensive then heat. In addition, desorbate is recovered at low purity [11].

1.1.4 Membrane Separations

Gas separation membranes are thin films that selectively transport gases through the membrane based on its permeability. The permeability is related as a function of membrane properties, the nature of the permeant species, and the interaction between them both. There are

many mechanisms that gas can transport through. For example, molecular diffusion, Knudsen diffusion, and surface diffusion. Nowadays, most membranes processes can handle to 250 MMSCFD. There are some new units that can also handle up to 500 MMSCFD. The key factors for membrane separation are intrinsic membrane permselectivity, ability of the membrane material to resist swelling induced plasticization and ability to process membrane material into beneficial asymmetric morphology with good mechanical strength under adverse thermal and feed mixture conditions [7].

1.1.4.1 Polymeric Membrane

Polymeric membranes have many commercial used. For example, recovery of nitrogen from air, separation of oxygen-nitrogen mixture and hydrocarbon in petrochemical industries and also, the purification of natural gas. The driving force for this separation is the pressure gradient across the membrane. There are two types of polymeric membranes that are commercially used in gas separations. Glassy and rubbery membranes. However, glassy membranes are more preferred due to its high selectivity and good mechanical properties. Polymeric membranes also have excellent intrinsic transport properties, high processability and low cost. On the other hand, even if polymeric membranes are known for their good properties, they have limit in a trade-off between permeability and selectivity [7].

1.1.4.2 Inorganic Membrane

Inorganic membranes (can also be called ceramic membranes) have good thermal, mechanical and chemical stability. They also have good erosion and bacteria resistance and a long operational life. Microporous and dense membranes are the types of ceramic membranes that are applicable for high-temperature gas purification applications. Dense membranes are made of polycrystalline ceramic materials. They are impermeable to all gases except for some limited

number of gases. But, their applications are not often used in gas separation processes due to its low permeability. Microporous membranes are made of glass, metal, alumina, zirconia, zeolite and carbon membranes. It gives high selectivity and permeability. However, the commercial applications of inorganic membranes are limited due to the lack of technology to form continuous membranes, high cost, its brittleness and challenges for sealing of membrane to module at high temperature.

1.1.4.3 Mixed Matrix Membrane

Mixed matrix membranes (MMMs) is considered to be the most practical approach with high potential for future applications. The molecular-sieve type fillers are used in MMMs such as zeolite and carbon molecular sieves are capable to separate between different molecules present in the feed mixture. The permeation in MMRs occurs by a combination of diffusion through the polymer phase and permeable zeolite particles. Based on the current trend, the market for separation of gas membranes are very small systems which its capacity is less than 5 MMSCFD, small systems with a capacity of 5 – 40 MMSCFD and medium to large systems which its capacity is more than 40 MMSCFD. Despite its high capital cost compared to amine plants, many membrane systems have been installed on offshore platforms [7].

To conclude membrane separations, they are mainly used for moderate-volume gas streams and have high concentration of CO_2. However, due to the cost of it, further development with higher selectivity, flux and cost effective is still needed.

1.1.5 Cryogenic Distillation

Cryogenic distillation or low-temperature distillation separation uses a very low temperature for purifying gas mixtures in the separation process. It is a type of extractive distillation. It differs from a normal distillation by the presence of a relatively non-volatile additive

put into the distillation column. The additive can be a mixture of butane, pentane and heavier components [12]. The process can be described in *Figure 4*, the natural gas is preconditioned and pre-cooling before entering the bulk column at -10 C and 40 bar. The concentration of CO_2 is greatly reduced in the bulk column. Then the purified gas will enter the second column which the temperature is also low. The LNG specification can be achieved in the third column which operates at 40 bar and -88 C. Then the gas is sent to customers or LNG productions. The CO_2 product from the bottom of the bulk column will be treated and recovered and send to re-injection in other wells and drilling site.

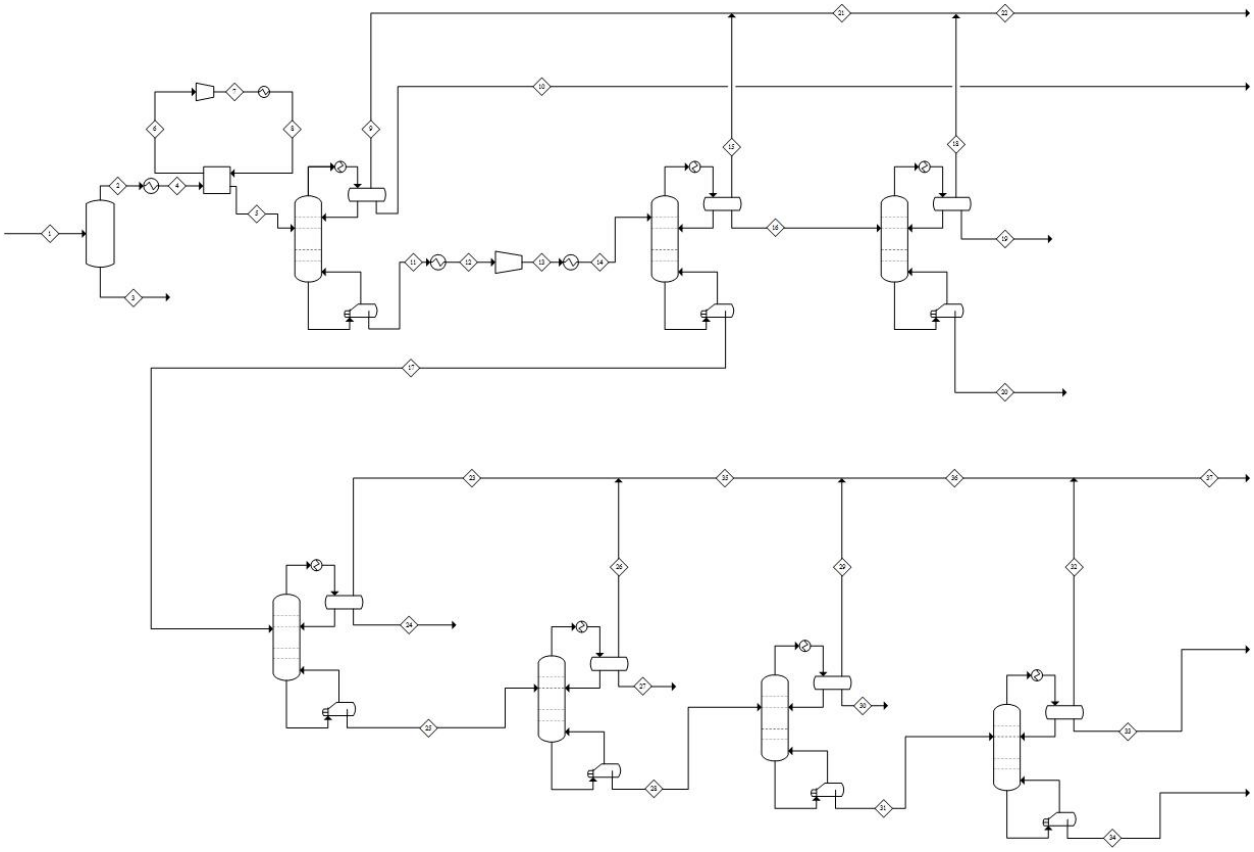

Figure 4: Cryogenic Distillation Process Overview [11]

The advantages of this process are that, the process is suitable for high concentration CO_2 gases and does not require compression for the CO_2 since there is no chemicals used. However, since the process is only efficient for high CO_2 concentration natural gases, if the natural gas fed to the process has a low concentration of CO_2, it will lower the whole plant efficacy. Moreover, the energy consumption for the process is relatively high comparing to other process commonly used in industry. Finally, the process temperature itself is very low. Thus, the possibility for process blockage due to freezing is high [7, 12].

1.1.6 Conclusion of all separations

The advantages and disadvantages are shown in Table 3.

Table 3: Comparison of Each Separation Process

Process	Advantages	Disadvantages
Absorption	- Process is commercialized - High purified product - Many chemical substance choices	- Not economical if physical solvent - Long time used for purification - Risk from chemicals
Adsorption	- High purity product - Adsorbent relocation to remote fields is simple	- Recovery of product is lower - Relatively single pure product - Relatively high energy usage
Membrane Separation	- Stability at high pressure - Less environmental impact	- Moderate purity - High capital cost - Recompression of permeate

Table 3 Continued

Process	Advantages	Disadvantages
Cryogenic Distillation	- Relatively higher recovery compared to other process - Relatively high purity products	- Highly energy intensive for regeneration - Not economical to scale down to small size - Unease operation due to its temperature and pressure

In general, pipeline specification for CO_2 is varied from each region in North America from 1% mol to 6 % mol of CO_2 [13]. There are only a few commercialized processes in the industry that is capable of reaching the CO_2 specification which are chemical absorption using amine as the absorber and physical absorption. Therefore, these two processes are considered in this project.

CHAPTER II

PROCESS SIMULATIONS AND COST EVALUATION

In the previous section, the processes chosen are amine absorption and physical absorption respectively. Therefore, to find the cost of each processes, a simulation is needed. The simulation tool chosen to model the processes is Aspen HYSYS V8.8 because it is the most suitable simulation for oil and gas processing due to its capability of dealing with unsteady state processes. Other approaches and simulations such as Aspen Plus or Pro/II can also be carried out for the following processes but may not give an accurate result as Aspen HYSYS. The gas flow rate from the production platform is 300.6 MMSCFD and the composition of the gas is shown in Table 4.

Table 4: Natural Gas Composition for Simulation

Compound	Mole %
Methane	69.380
Ethane	5.320
Propane	1.770
i-Butane	0.420
n-Butane	0.520
n-Pentane	0.210
Water	3.85
Carbon Dioxide	13.150
Hydrogen Sulfide	0.334
Nitrogen	2.05

2.1 Amine Absorption process

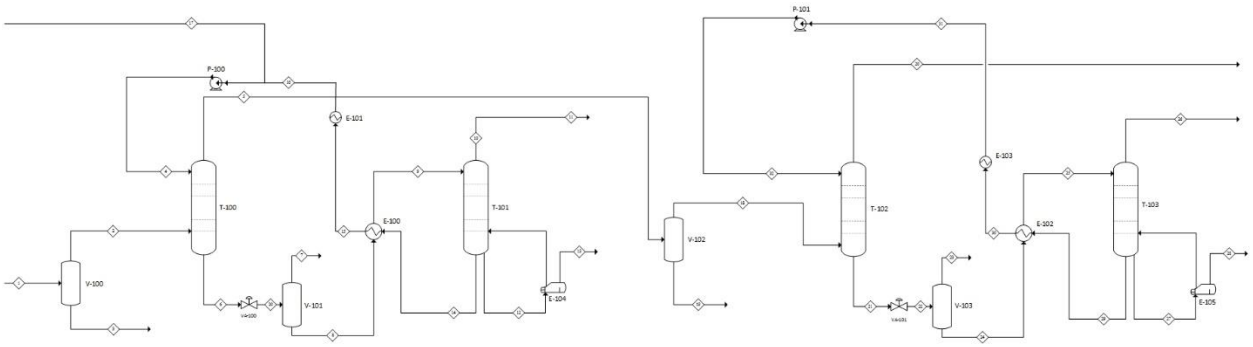

Figure 5: Amine Absorption Process [3]

Amine absorption process is shown in Figure 5. The process is separated into two different sections. The first section is the CO_2 sweetening part. The gas from the well or drilling site will go through a separator and is pass to the absorber column. The absorbent used to remove CO_2 and also H_2S out of the natural gas is methydiethanolamine (MDEA) because it consumes less energy than other amines [3] and as already pointed out in chapter 1, all amines should give the similar cost. Then the gas is sent from the top stream of the column to the second section. The bottom product of the absorber column is to be regenerated by a stripper column. The second section is the dehydration part. Because the best condition for transporting natural gas is to send it at dew point, the water content of the sales gas is needed to be controlled. Therefore, the gas will have to pass a glycol contractor which the water removal agent used is diethylene glycol [14]. The second tower of the contacting part is similar to the first section, a regenerator used to recycle the glycol. Then the gas at the top of the first column will be send to a compressor to be compress to the shore or customers' end.

Simulations were done for the amine absorption process, and since the CO_2 pipeline specification is between 1 to 6 percent mole, the sales gas final concentration is varied between this range of concentration with an interval of 0.5. The fluid package used is amine package for the amine section and glycol package for the water removal section.

The amine feed flow and the sales gas flow of each concentration from the simulation can be summarized in the following table, assuming the gas price is 3.3 USD per MMBTU [14].

Table 5: Sales Gas Summarization for Amine Absorption Process

CO_2 Final Concentration (mol%)	**Sales Gas Flow (MMBTU)**	**Amine Feed Flow (m^3/h)**	**Revenue (100 Million USD)**
1	247416	3420	270
1.5	249392	2835	273
2	251056	2458	274
2.5	252824	2135	276
3	254384	1900	278
3.5	256048	1665	280
4	257608	1506	282
4.5	259168	1366	284
5	260624	1265	285
5.5	262184	1158	287
6	263744	1069	289

From the data in Table 5, a relationship between the amine feed flow to absorbers and the CO_2 final concentration in the sales gas can be plotted as shown in Figure 6,

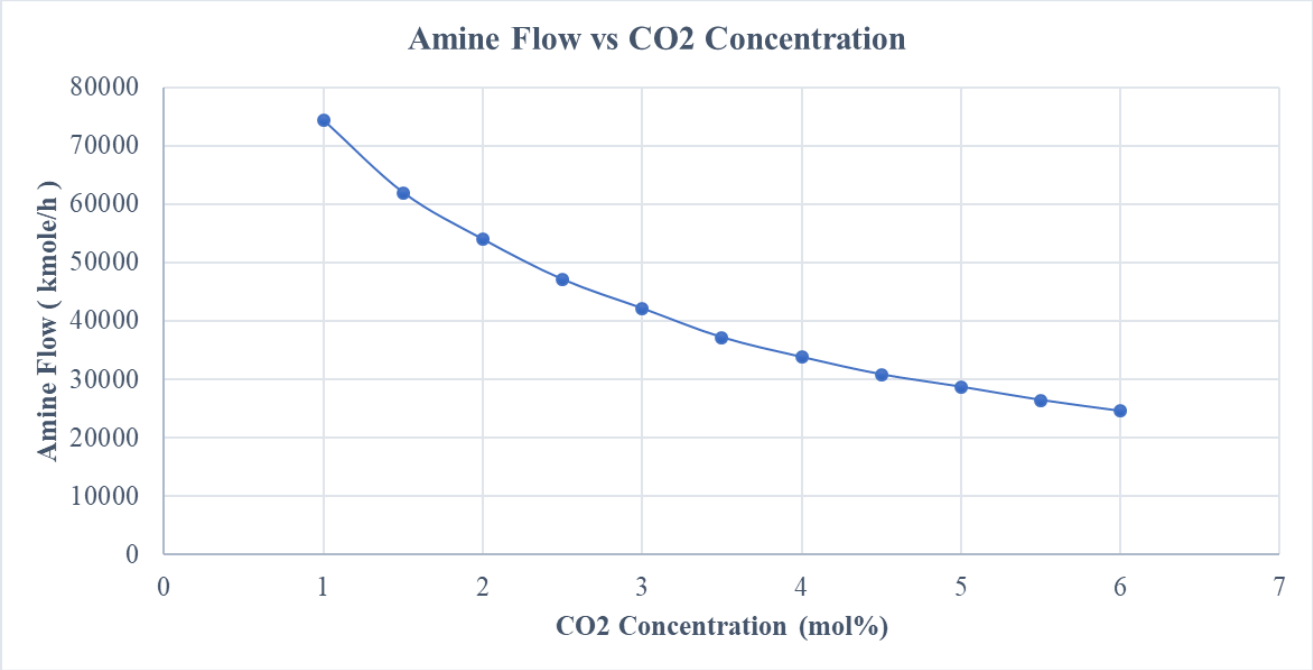

Figure 6: Relationship Between Amine Feed Flow and CO_2 Final Concentration

Figure 6 indicates that the amine feed flow is higher as the CO_2 final concentration reduces. However, the relationship between the two variables is not linear. The less CO_2 concentration needed, the amine feed flow tends to increase exponentially. Thereby, the cost of the amine will be higher for lower CO_2 concentration natural gas. As for the capital cost, the equipment were evaluated using the lowest concentration at 1% mol. The reason is because at this condition, the equipment can perform to remove any other required specification above 1% and it can be fixed for every pipeline length. On the other hand, the operating cost of the process depends on how

much CO_2 is removed. The operating cost obtained from Aspen Economics Analyzer for each case is shown in Table 6,

Table 6: Amine Absorption Operating Cost for each CO_2 Concentration

CO_2 Final Concentration (mol%)b	**Total Operating Cost (Million USD)**
1	168
1.5	154
2	145
2.5	139
3	135
3.5	131
4	128
4.5	125
5	123
5.5	121
6	119

Then the relationship between the concentration and the operating cost of the process can be generated in Figure 7.

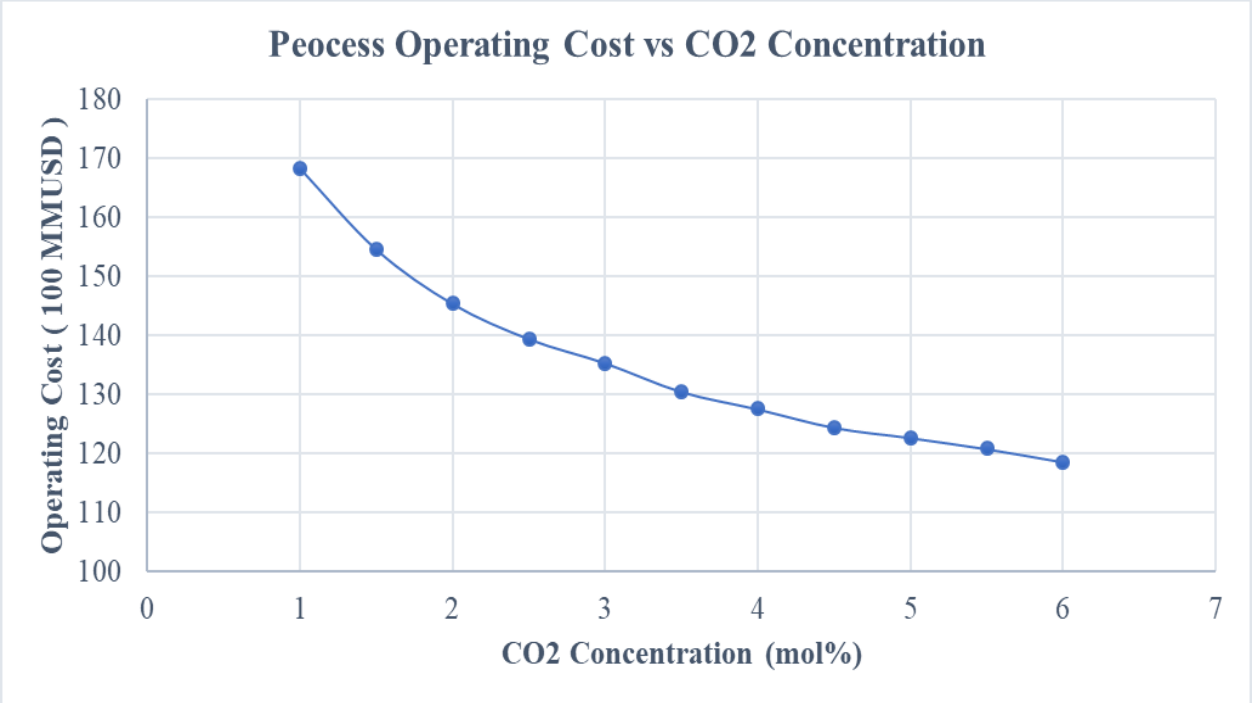

Figure 7: Relationship Between the Amine Absorption Operating Cost and CO_2 Final Concentration

The relation corresponds to the relationship between the amine flow and the CO_2 concentration. As the operating cost goes higher, the CO_2 final concentration that is removed is lower. Furthermore, the relationship is not linear similarly to the previous relationship. Thus, as the interval of gas purity rises (e.g. comparing from 5% to 6% and from 2% to 3%), the difference between the cost is larger.

Therefore, in this section, the total process cost is higher as the CO_2 removal increases. However, the decision for the most suitable concentration still cannot be decided because the pipeline cost from corrosion is still not considered which both will be discussed in the next section.

2.2 Selexol Process

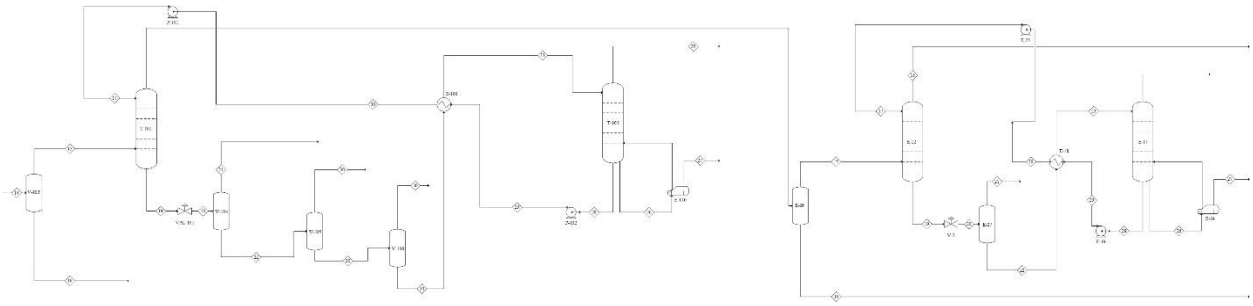

Figure 8: Physical Absorption Process by using Selexol as Solvent

Selexol process is shown in Figure 8 [15]. The process resembles the amine absorption process. However, the absorbent is totally different. The absorbent chosen to be used in this process is selexol because it is the most common physical solvent used in the industries. It is a physical absorber which will not react chemically with the gas but still, it can remove the CO_2 to the required specification. The gas enters the absorber column then the gas which the CO_2 is removed will leave the top of the column. The bottom product is the solvent with high CO_2 concentration. Another difference from the amine absorption part is that after the rich solvent leaves the bottom of the absorber, it goes through three two-phase separators to remove the residual gas. This is because it is more difficult to regenerate the solvent if there is too much gas in the stream unlike amine absorption. The gas from the top of the column then goes through the glycol contactor the same as the amine process to remove some of the water out of the gas to make the gas ready for transportation to the customers' end.

Simulations were also performed for physical absorption process with the same CO_2 concentration range at 1 to 6 % mole and interval. The solvent used in this process is selexol

because it is one of the most common physical solvent used in industries. Moreover, the cost of selexol is not high.

The selexol feed flow and the sales gas flow of each concentration can be summarized in Table 7, assuming the gas price is 3.3 USD per MMBTU [14].

Table 7: Sales Gas Summarization for Physical Absorption Process

CO_2 Final Concentration (mol%)	**Sales Gas Flow (MMBTU)**	**Selexol Feed Flow (m^3/h)**	**Revenue (100 Million USD)**
1	209872	5607	229
1.5	215800	4732	236
2	219544	4314	240
2.5	223392	3945	245
3	226616	3662	248
3.5	229632	3407	251
4	232232	3212	254
4.5	234832	3022	257
5	235465	2849	258
5.5	237016	2617	259
6	241696	2537	265

The relationship between selexol flow and CO_2 concentration can be generated in Figure 9.

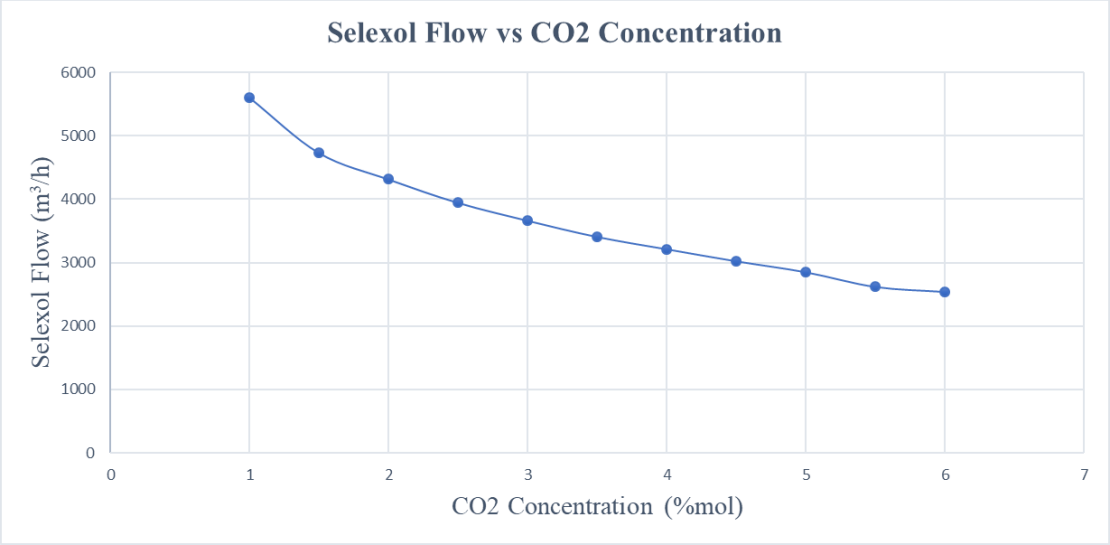

Figure 9: Relationship Between Selexol Feed Flow and CO2 Final Concentration

From Figure 9, the relationship between the selexol flow and CO_2 concentration is close the relationship of the amine absorption flow. The increasing the removal of the CO_2 gives higher selexol flow. Moreover, the relationship is more linear as it is thna the amine absorption case in the previous section. However, the results are still similar. The capital cost is also the same for this case, fixed at the lowest CO_2 concentration which is 1%. Therefore, the selexol process operating cost can be summarized in Table 8.

Table 8: Physical Absorption Operating Cost for each CO2 Concentration

CO_2 Final Concentration (mol%)	**Total Operating Cost (Million USD)**
1	120
1.5	99
2	86
2.5	84
3	82
3.5	79
4	76
4.5	75
5	71
5.5	70
6	67

From Table 8, the relationship between the solvent flow and CO_2 concentration can be generated in Figure 10.

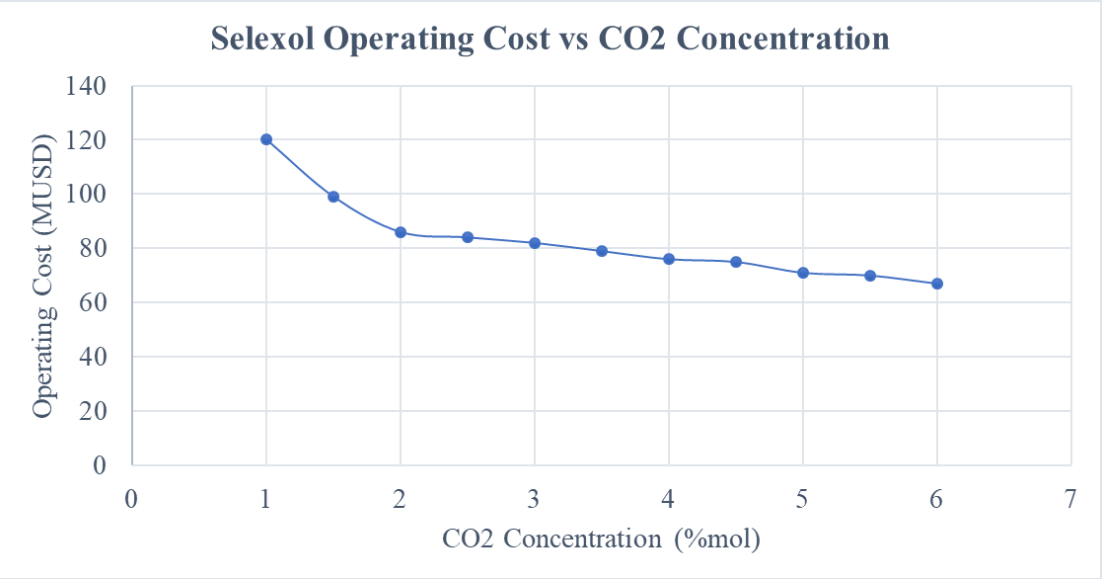

Figure 10: Relationship Between the Physical Absorption Operating Cost and CO2 Final Concentration

The relation corresponds to the relationship between the amine flow and the CO_2 concentration. As the operating cost goes higher, the CO_2 final concentration that is removed is lower. However, the plot does not look the same as the amine absorption process. From the range of 2% to 6%, the plot is close to linear. However, at really low CO_2 concentration (1% and 1.5%), the cost increases not linearly but exponentially. This may indicate that at too high CO_2 removal rate, the process operating cost might be too high to become optimal. Likewise, the suitable CO_2 concentration still cannot be decided to be the same as the amine absorption case. The process operating cost must be combined with the corrosion analysis and pipeline cost which will be evaluated in the next chapter.

CHAPTER III

CO_2 CORROSION AND PIPELINE COST EVALUATION

Carbon dioxide corrosion was first found in documentations in the 1940s and there have been many studies follow the work. The following is the reaction equilibrium of how CO_2 corrosion occurs.

$$CO_2 + H_2O \longleftrightarrow CO_2 \text{ ---------- } \sim H_2CO_3 \longleftrightarrow H^+ + HCO_3^- \quad (5)$$

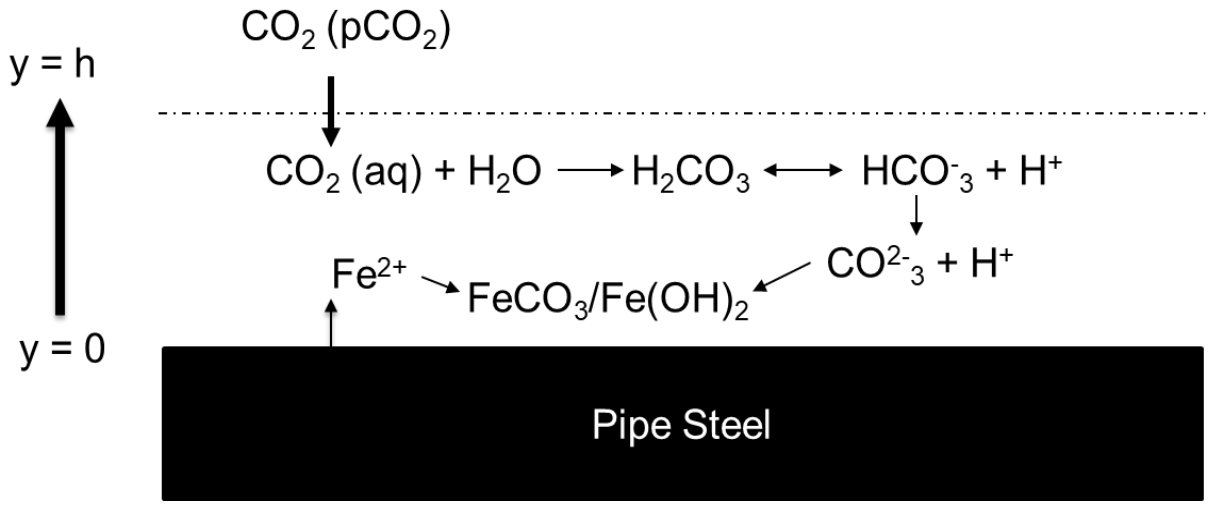

Figure 11: CO_2 Corrosion in Pipe Steel [16]

Figure 11 summarized how carbon dioxide corrosion occurs on the surface of metal. The presence of CO_2 in the stream gives a partial pressure of CO_2 (P_{CO2}) which eventually dissolves in the aqueous phase. It reacts with water to form carbonic acid (H_2CO_3). Then carbonic acid dissociates into two ions, bicarbonate and hydrogen ion. The bicarbonate ion further separated into carbonate and hydrogen ion. Finally, the reaction of carbonate and ferrous ion will result in the formation of ferrous carbonate ($FeCO_3$).

3.1 Damages from CO2 Corrosion

Usually, carbon dioxide corrosion is uniform corrosion. It can cause three forms of localized attack which are mesa-type attack, pitting and flow-induced corrosion [17].

3.1.1 Mesa-type attack

A form of localized corrosion that takes place in low to medium fluid-flow environment in production wells is called mesa-type attack.

3.1.2 Pitting

Pitting is a form of localized corrosion which often happens in low-velocity fluid flow environment around dew point temperatures in an oil and gas-producing well. It caused holes in the metal surface. Low to medium velocity fluid flow is still capable of washing away any protective films formed on the metal surfaces.

3.1.3 Flow- induced Localized Corrosion

This is another form of localized corrosion which often starts from pits that had previously been sites of localized mesa attack. This form of corrosion is highly dependent on high fluid flowrates.

3.2 CO_2 corrosion models

There are several companies and academic institutes that approached to develop CO_2 corrosion models which are suitable for any conditions. Thsee are the models developed in industries.

3.2.1 The 1975 De Waard-Milliams Correlation

This is a model developed by de Waard and coworkers [18]. The first version of it depends on the temperature and the CO_2 partial pressure only. Later, there has been several developments to the model and different correction factors have been added to improve the model. The model includes an on/off factor for oil wetting crude oil systems. The model also includes pH calculation

only for pure condensed water or condensed water saturated with corrosion products. However, the model has little sensitivity to the variation of pH.

3.2.2 NORSOK M-506 Model

This model is an empirical model developed by the Norwegian oil company called Statoil, Norsk Hydro and Saga Petroleum [19]. The model is fitted to a same data as the De Waard-Milliams model but in addition, includes more recent experiment results at 100 to 150 C as well. The model also takes the effect of protective corrosion films at high temperature and pH. The model is more sensitive to the change of pH compare to the de-Waard model.

3.2.3 HYDROCOR Model

This model was developed by Shell to combine corrosion and fluid flow modeling [20]. The model is a combination between different CO_2 corrosion models for multiphase flow, pH calculation and iron carbonate precipitation.

3.2.4 CORPLUS Model

CORPLUS is developed by Total [19]. It is an integration between the Cormed tool and Lipucor model. This model is based on detailed analysis of the water chemistry including the effects of organic acids, calcium and also CO_2 itself. It gives no protection from corrosive films or oil wetting.

3.2.5 Cassandra Model

BP is the company who develop this model. In this model, pH calculation is included while pH value is evaluated from the CO_2 content. The effect of protective films can be included or excluded by the user choosing the scaling temperature. Thus, the model does not give that much

credit for protective films at high temperature. Also, oil wetting effects are not included in this model [21].

3.2.6 KSC Model

The model is a mechanistic model for CO_2 corrosion. This model takes into account the protective corrosion films. It is developed at the Institute of Technology. The model is based on an electrochemical model by combining it with a transport model. It has a strong effect of protective corrosion films which is sensitive to pH and temperature. Therefore, when there is high temperature and high pH, the model tends to lean toward low corrosion rate [22].

3.2.7 Multicorp

Ohio University put an effort to generate this model. This model was based on the KSC model using mechanistic modeling of the chemical, electrochemical and transport. It has been developed further at the university by considering also the effect of multiphase flow, precipitation of iron carbonate films and effects of oil wetting and crude oil chemistry. The model is based on modeling of kinetics of chemical reactions in the bulk and electrochemical reactions at the steel surface and many others. However, the model is correlated large against a large amount of laboratory data and some of the field data [19].

3.2.8 ECE Model

ECE model was developed by Intetech also based on the de Waard Model. It includes a module calculation of pH from the water chemistry and bicarbonate produced by the corrosion. However, there is chance that it may calculate higher pH than the actual value. It also considers the H_2S effects [19].

3.2.9 Predict Model

A model by InterCorr International, now part of Honeywell. This model is again based on the de Waard Model with different correction factors. The model has very strong effects of oil wetting and variation of pH. Moreover, this model includes a flow modeling module for evaluating the flow velocity and regime. The model tends to give low rates if pH goes beyond 4.5 [19].

3.2.10 Tulsa Model

Developed by University of Tulsa, it is a two-phase flow mechanistic model considering also the kinetics of electrochemical reactions and mass transfer. The effect of protective corrosion films is very high in the model and sensitive to change of pH value [19].

3.2.11 ULL Model

University of Louisiana at Lafayette developed this model firstly to work on gas condensate wells. The model determines the temperature and pressure profiles, phase equilibrium and flow behaviors. It also has a strong effect on oil wetting when condensation of hydrocarbon happens [19].

3.2.12 CorPos Model

This model is developed by CorrOcean now known as Force Technology where the combination of multiphase flow estimation together with water chemistry calculation and a point corrosion model are used in order to evaluate the pH and eventually, the corrosion rate. The model though gives low corrosion rate to a very low water cut stream [19].

3.2.13 OLI Model

Model developed by OLI systems. This model is a mix between the thermodynamic model for the concentration of molecular and ionic species of systems with electrochemical corrosion

model. The model is a mechanistic model of the phase behavior and many reactions. Nevertheless, the model does not include any effect of oil wetting [19].

3.2.14 SweetCor Model

The SweetCor corrosion model was developed by once again, Shell from a large database of corrosion data in laboratories. The model includes a various range of CO_2 partial pressure, temperatures and flows. It does not take any effect of oil wetting into consideration. Almost independent of pH [19].

3.3 Conclusion and selection of all the corrosion models

Even though there are various models in the industries, there are only few models that are not owned by companies and are available for public usage. The models are de Waard, NORSOK, CORPLUS, KSC and Abbas model [17, 19, 20, 21, 22]. The comparison of each corrosion models is shown in Table 9.

Table 9: Corrosion Model Conclusion

Model	Characteristics	Temp	Pressure	Fugacity CO_2 (bar)	Shear Stress (Pa)	pH	Glycol (% mass)	Inhibitor Efficacy	Open to Public
NORSOK Model	Fitted to large amount of experimental data and also effective for high temperature and pH	20 - 150	1 - 1000	0.1 - 10	1 - 150	3.5 - 6.5	0 - 100	0 - 100	Yes
de Waard Model	A common method based on empirical fitting lab experiments. Takes little account regarding protective films	0 - 140	0 - 200	0.01 - 10	-	3.0 - 5.0	-	-	Yes
Cassandra	Similar to de Waard. Considered oil wetting effect but weak high temperature model	-	-	-	-	-	-	-	No
HYDROCOR	Not suitable for gas system	Max 150	-	Max 20	-	-	-	-	No
CORPLUS	Suitable for large amount of organic acids, calcium large amount of field data	Max 150	-	0.05 - 10	-	>5.6	-	-	Yes
KSC	Simulates electrochemical and chemical reactions and diffusion of corrosive species	Max 150		Max 20					Yes

From Table 9, the NORSOK model has a high range of temperature and pH whereas the Abbas Model has a wide range of CO_2 fugacity and other models are lacking information in the range of operating conditions the model is capable of evaluating the corrosion rate. Therefore, from the information given, the NORSOK model is chosen to evaluate the corrosion rate in the pipelines.

3.4 NORSOK Model

The NORSOK corrosion model is a model used for calculating corrosion rate in hydrocarbon processing and process systems where the cause is CO_2. The model in general is based on flow-loop experiments at the range temperature of 5 to 160 C. The variables used for example, are CO_2 fugacities, pHs and wall shear stress. The following equations are used to calculate the corrosion rate [23].

For 20 to 150 C

$$\mathrm{CR_t} = 0.00476421 \times \mathrm{K_t} \times \mathrm{S} + 0.0324 \log(\mathrm{f_{CO_2}}) \times \mathrm{f(pH)T} \quad (6)$$

For 15 C

$$\mathrm{CR_t} = 0.0001 \times \mathrm{K_t} \times \mathrm{S} + 0.0324 \log(\mathrm{f_{CO_2}}) \times \mathrm{f(pH)T} \quad (7)$$

For 5 C

$$\mathrm{CR_t} = 0.36 \times \mathrm{K_t} \times \mathrm{f_{CO_2}} \times \mathrm{f(pH)T} \quad (8)$$

All the corrosion rates are expressed as mm/year. The value of $\mathrm{K_t}$ differs by the temperature. Table 10 below gives the value of it.

Table 10: K_t for each Range of Temperature

Temperature	K_t
5	0.42
15	1.59
20	4.762
40	8.927
60	10.695
80	9.949
90	6.250
120	7.770
150	5.203

The pH function is also given in Table 11.

Table 11: pH functions for each range of temperature and pH

Temperature	pH	f(pH)
5	$3.5 < pH < 4.6$	$f(pH) = 2.0676 – (0.2309pH)$
5	$4.6 < pH < 6.5$	$f(pH) = 4.342 – 1.051pH + 0.0708pH^2$
15	$3.5 < pH < 4.6$	$f(pH) = 2.0676 – (0.2309pH)$
15	$4.6 < pH < 6.5$	$f(pH) = 4.986 – 1.191pH + 0.0708pH^2$

Table 11 Continued

Temperature	pH	f(pH)
20	3.5 < pH < 4.6	f(pH) = 2.0676 – (0.2309pH)
20	4.6 < pH < 6.5	$f(pH) = 5.1885 – 1.2353pH + 0.0708pH^2$
40	3.5 < pH < 4.6	f(pH) = 2.0676 – (0.2309pH)
40	4.6 < pH < 6.5	$f(pH) = 5.1885 – 1.2353pH + 0.0708pH^2$
60	3.5 < pH < 4.6	f(pH) = 1.836 – (0.1818pH)
60	4.6 < pH < 6.5	$f(pH) = 15.444 – 6.1291pH + 0.8204pH^2$
80	3.5 < pH < 4.6	f(pH) = 2.6727 – (0.3636pH)
80	4.6 < pH < 6.5	$f(pH) = 331.68 \times e^{(-1.2618pH)}$
90	3.5 < pH < 4.57	f(pH) = 3.1355 – (0.4673pH)
90	4.57 < pH < 5.62	$f(pH) = 21254 \times e^{(-2.1811pH)}$
90	5.62 < pH < 6.5	f(pH) = 0.4014 – (0.0538pH)
120	3.5 < pH < 4.3	f(pH) = 1.5375 – (0.125pH)
120	4.3 < pH < 5	f(pH) = 5.9757 – (1.157pH)
120	5 < pH < 6.5	f(pH) = 0.4014 – (0.0538pH)
150	3.5 < pH < 3.8	f(pH) = 1
150	3.8 < pH < 5	$f(pH) = 17.634– 7.0945pH + 0.715pH^2$
150	5 < pH < 6.5	f(pH) = 0.037

Apart from the main variables used in the three corrosion equations above, there are some other input parameters needed to be determined to evaluate the rate.

3.4.1 Wall Shear Stress

This parameter is required to calculate the corrosion rate. The equation used is:

$$S = 0.5 \times \rho_m \times f \times u_m^2 \tag{9}$$

Where the shear stress is in Pascal.

The friction factor f can be expressed as:

$$f = 0.001375 \left[1 + \left(20000 \frac{k}{D} + 10^6 \frac{\mu_m}{\rho_m u_m D}\right)^{0.33}\right] \tag{10}$$

In the expression there are mixture density, velocity and viscosity which are expressed as:

$$\rho_m = \rho_L \lambda + \rho_G (1 - \lambda) \tag{11}$$

$$\rho_L = \phi \rho_w + \rho_o (1 - \lambda) \tag{12}$$

$$\rho_G = 2.7\ 14.5\ 16.018\ P \frac{\text{specific gravity}}{Z(460 + T_f)} \tag{13}$$

$$u_m = u_L^s + u_G^s \tag{14}$$

For Liquid Flow rate:

$$u_L^s = \frac{Q_L}{A} \tag{15}$$

Gas Superficial velocity:

$$u_G^s = \left(\frac{Q_G}{A}\right) Z\left(\frac{T}{T_{std}}\right) \tag{16}$$

$$\mu_m = \mu_L \times \lambda + \mu_G \times (1 - \lambda) \tag{17}$$

$$\lambda = \frac{Q_L}{Q_L + Q_G} \tag{18}$$

If water is present the viscosity is found as follows:

$$\mu_L = \mu_0 \left(1 + \frac{\frac{\phi}{K_0}}{1.187 - \frac{\phi}{K_0}} \right)^{2.5} \tag{19}$$

The value of K_0 for the maximum relative viscosity μ_{relmax} (relative to the oil) and corresponding watercut at the inversion point ϕ_C is equal to:

$$K_0 = \frac{\phi_C}{1.187 \left(1 - \left(\frac{1}{\mu_{relmax}} \right)^{0.4} \right)} \tag{20}$$

If it is not known, medium viscosity oil and water dispersion will be used instead. The maximum relative viscosity is 7.06 at a watercut of 0.5. The oil viscosity is 0.0011 at 60 C and similarly, the water viscosity is 0.00046.

Above the inversion point, the viscosity of any dispersion is given as:

$$\mu_L = \mu_W \left(1 + \frac{\frac{1-\phi}{K_w}}{1.187 - \frac{1-\phi}{K_w}} \right)^{2.5} \tag{21}$$

Where

$$K_w = \frac{1 - \phi_C}{1.187 \left(1 - \left(\frac{R}{\mu_{rel/max}} \right)^{0.4} \right)} \tag{22}$$

The viscosity of water in the temperature range of 0 to 20 C is:

$$\mu_w = 10^{\frac{1301}{998.333 + 8.1855(T_c - 20) + 0.00585(T_c - 20)^2} - 1.30233} \cdot 10^{-3} \tag{23}$$

For 20 to 100 C (can be used to 150 C but not as accurate)

$$\mu_w = 1002 \left(10^{\frac{1.3272(20 - T_c) - 0.001053(T_c - 20)^2}{T + 105}} \right) \cdot 10^{-3} \tag{24}$$

For the medium viscosity oil at 60 C, R is equal to 0.42

3.4.2 Fugacity of CO_2

Another significant parameter for evaluating the corrosion rate is the CO_2 fugacity. As gas is not ideal at high pressure, the real CO_2 pressure or fugacity can be expressed as:

$$f_{CO_2} = a \times p_{CO_2} \tag{25}$$

The partial pressure of CO_2 can be found by

$$p_{CO_2} = \left(\frac{\text{mole\% } CO_2 \text{ in the gas phase}}{100\%}\right) \times P \tag{26}$$

Or

$$P_{CO_2} = \frac{\text{mass flow of } CO_2 \text{ in the gas phase } \left(\frac{\text{kmole}}{\text{h}}\right)}{\text{total mass flow in the gas phase } \left(\frac{\text{kmole}}{\text{h}}\right)} \times P \tag{27}$$

The fugacity coefficient is given as:

$$a = 10^{P\times\left(0.0031-\frac{1.4}{T}\right)} \text{ for } P \leq 250 \text{ bar} \tag{28}$$

$$a = 10^{250\times\left(0.0031-\frac{1.4}{T}\right)} \text{ for } P > 250 \text{ bar} \tag{29}$$

3.4.3 pH Calculations

The pH calculation is based on several chemical reactions and equilibrium constants. The reactions are as follow:

$$CO_2\,(g) \leftrightarrow CO_2\,(aq) \qquad K_1 = \frac{[CO_2]}{p_{CO_2}} \tag{30}$$

$$CO_2\,(aq) + H_2O \leftrightarrow H_2CO_3 \qquad K_2 = \frac{[H_2CO_3]}{[CO_2]} \tag{31}$$

$$H_2CO_3 \leftrightarrow H^+ + HCO_3^- \qquad K_3 = \frac{[HCO_3^-][H^+]}{[H_2CO_3]} \tag{32}$$

$$HCO_3^- \leftrightarrow H^+ + CO_3^- \qquad K_4 = \frac{[CO_3^{2-}][H^+]}{[HCO_3^-]} \tag{33}$$

$$H_2O \leftrightarrow H^+ + OH^- \qquad K_5 = [H^+][OH^-] \tag{34}$$

In this NORSOK model, the system has to be electro-neutral which can be expressed as:

$$[Na^+] + [H^+] = [HCO_3^-] + 2[CO_3^{2-}] + [OH^-] + [Cl^-] \quad (35)$$

The model assumes that bicarbonate is added as sodium bicarbonate ($NaHCO_3$) and there is no other salt than sodium chloride (NaCl) present in the solution. Then the salt will dissolve as:

$$NaCl \quad Na^+ + Cl^- \quad (36)$$

$$NaHCO_3 \leftrightarrow Na^+ + HCO_3^- \quad (37)$$

Based on all the assumptions, the balance for the bicarbonate is as follow:

$$[\text{Initial Bicarb}] = [Na^+] - [Cl^-] \quad (38)$$

The combination of the equations for the equilibrium constant, the electro-neutrality equation and the mass balance for bicarbonate is the equation for the hydrogen cation:

$$[H^{+3}] + [\text{Initial Bicarb}][H^{+2}] - (K_H K_1 K_2 p_{CO_2} + K_w)[H^+] - 2K_H K_1 K_2 K_3 p_{CO_2} = 0 \quad (39)$$

The equation can be solved using numerical method. Also, the pH in a condensed water system saturated with iron carbonate can also be calculated. It will generally become:

$$\left(\frac{2K_{SP}}{K_H K_1 K_2 K_3 p_{CO_2}}\right)[H^{+4}] + [H^{+3}] + [\text{Initial Bicarb}][H^{+2}] - (K_H K_1 K_2 p_{CO_2} + K_w)[H^+] - 2K_H K_1 K_2 K_3 p_{CO_2} = 0 \quad (40)$$

Which this equation can also be solve by numerical approaches.

For the equilibrium constant K_{SP}. It is shown in the following equation:

$$K_{SP} = 10^{-(10.13 + 0.0182 T_C - 2.44 I^{0.5} + 0.72 I)} \quad (41)$$

For a temperature range of 0 to 80 C

$$K_H = 55.5084\ e^{-\left(4.8 + \frac{3934.4}{T_K} - \frac{941290.2}{T_K^2}\right)} 10\text{^} - (1.790 \cdot 10^{-4} P + 0.107 I) \quad (42)$$

For a temperature of 80 to 200 C

$$K_H = 55.5084\ e^{-\left(\frac{1713.53\left(1 - \frac{T_K}{647}\right)^{\frac{1}{3}}}{T_K} + 3.875 + \frac{3680.09}{T_K} - \frac{1198506.1}{T_K^2}\right)} 10\text{^} - (1.790 \cdot 10^{-4} P + 0.107 I) \quad (43)$$

For the ions dissociation carbonic acid and CO_2 are based on the following equations:

$$K_2 = 10^{-\left(356.3094+0.06091964T_K-\frac{21834.37}{T_K}-126.833\log T_K+\frac{168491.5}{T_K^2}-2.564\cdot10^{-5}P-0.491I^{0.5}+0.379I-0.06506I^{1.5}-1.458\cdot10^{-3}IT_f\right)} \quad (44)$$

$$K_3 = 10^{-\left(107.8871+0.0325249T_K-\frac{5151.79}{T_K}-38.92561\log T_K+\frac{563713.9}{T_K^2}-2.118\cdot10^{-5}P-1.255I^{0.5}+0.867I-0.174I^{1.5}-1.588\cdot10^{-3}IT_f\right)} \quad (45)$$

Also, the equilibrium constant for dissociation of water is:

$$K_w = 10^{-\left(29.3868-0.0737549T+7.47881\times10^{-5}T^2\right)} \quad (46)$$

Various input parameters have to be put in the equations to find the corrosion rate. However, in the NORSOK model, those parameters have its own range that it is applicable in the equations. Table 12 shows the range of the parameters for evaluating the wall shear stress.

Table 12: Parameters Limits for Evaluating the Wall Shear Stress

Parameter	Units	Range	Other Comments
Temperature	C	20 – 150	
Total Pressure	Bar	1 – 1000	
Total Mass Flow	Kmole/h	10^{-3} - 10^{8}	Reynolds number must be higher than 2300
CO_2 fugacity in the gas phase	Bar	0.1 – 10	Reynolds number must be higher than 2300
Wall Shear Stress	Pa	1 – 150	
pH		3.5 – 6.5	

Table 12 Continued

Parameter	Units	Range	Other Comments
Inhibitor efficiency	%	0 - 100	Reynolds number must be higher than 2300
Roughness	μm	0 – 100	Default Value = 50
Compressibility		0.8 – 1	Default Value = 0.9
Specific Gravity of Gas Relative to Air		0.5 – 1	Default Value =0.8
Water Density	Kg/m^3	995 – 1050	Default Value = 1024
Oil Density	Kg/m^3	600 – 1100	Default Value = 850
Gas Density	Kg/m^3	1 – 1700	
Water Viscosity	cP	0.17 – 1.1	
Oil Viscosity	cP	0.2 – 200	Default Value = 1.1
Gas Viscosity	cP	0.02 – 0.06	Default Value = 0.03
Water Cut at inversion Point		0.3 – 0.9	Default Value = 0.5
Maximum Relative Liquid Viscosity		1 - 100	Default Value = 7.06

Table 13 shows the range for the input parameters for pH calculations

Table 13: Parameter Limits for Determining the pH

Parameter	Units	Range	Other Comments
Temperature	C	5 - 150	
Total Pressure	bar	1 - 1000	
Total Mass Flow	Kmole/h	$10^{-3} – 10^{6}$	
CO_2 Fugacity	bar	0 - 10	Depends on total pressure
Bicarbonate	mg/l	0 - 20000	
Ionic Strength/Salinity	g/l	0 - 175	

From all the equations given above, the determination of the corrosion rate for usage in the other section can be obtained.

3.5 CO_2 Inhibitor

From the previous section, the corrosion rate is between 8.6 and 22 millimeters per year resulted in a very high-thickness pipeline. For example, if the corrosion rate is 22 millimeters per year, then if the plant is designed to have a 10 years lifetime, the thickness of the pipe would have to be more than 220 mm per year which there are no pipes in industry that have such a large thickness [24]. Therefore, a CO_2 corrosion inhibitor will have to be implement in the pipeline to avoid the corrosion damage to the pipe. The mechanism of CO_2 inhibition is first, absorption on the metal surface. Then secondly, the inhibitor changes the wettability of the metal surface, so it is not contacted with water. Finally, changing the oil- water interfacial tension. Film-forming corrosion inhibitors are the most commonly used to control the steel surface inner parts of the pipeline. The inhibitors used in oil and gas industries are mostly formed of organic chemical compounds. These compounds form thin film on the surface of the pipe steel which will eventually decrease the corrosion rate from the CO_2 and other substances that may cause corrosion [25]. There

are many kinds of inhibitors that are available in industries. Proprietary mercaptoalcohol (MA) is one of the most general inhibitors. Sodium thiosulfate, thiourea, thioglycolic acid (TGA), L-cystein, 3,3 -dithiodipropionic acid (DTDPA), imidazoline, Potassium nitronated and tertiary butyl mercaptan (t-BM) can also be obtained from various commercial sources. The corrosion inhibitors efficiency can be tested by two different ways; Rotating cylinder electrode (RCE) and flow loop (FL) tests. Both tests will give out the corrosion rate after the implementation in the test subject which there are many works that gave out results [26]. The corrosion inhibitor should be chosen based on the gas' pH and temperature and also the condition of the pipeline surface for example, the type of pipeline used. However, corrosion inhibitors information in industries are confidential and the cost is mostly unknown. The corrosion chosen in this project was imidazoline due to many works regarding the performance of imidazoline were available in public and in MKOPSC. Another corrosion considered was MA, However, due to its confidentiality, it was dismissed.

The next step is to evaluate how much CO_2 inhibitor is needed. It can be determined by using the relationship between the corrosion inhibition efficiency and the corrosion concentration in the gas stream which can be shown in

Figure 12.

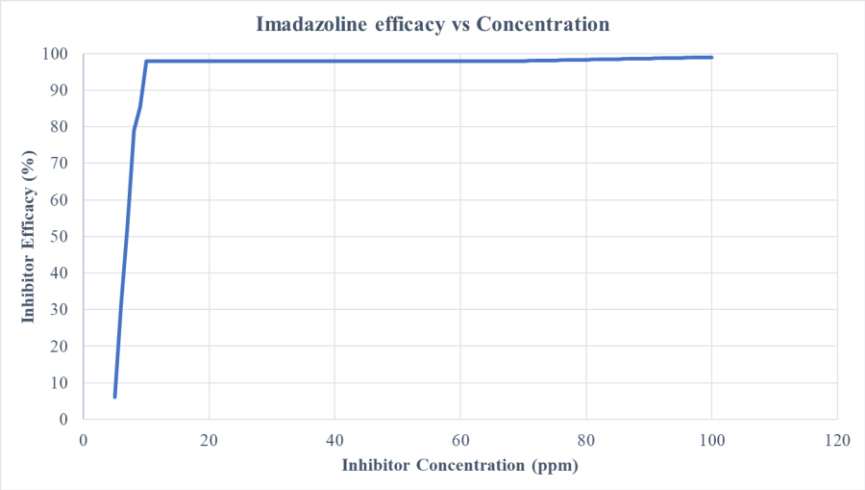

Figure 12: Relationship between the Corrosion inhibitors Efficacies and its Concentration [26]

For example, if the inhibitor used is imidazoline, and the required efficiency is 90%, the concentration of the inhibitor in the gas would have to be about 10 ppm. Using this relationship, the amount of inhibitor can be obtained and can be used for further cost analysis in the next section

3.6 CO_2 Pipe Corrrosion

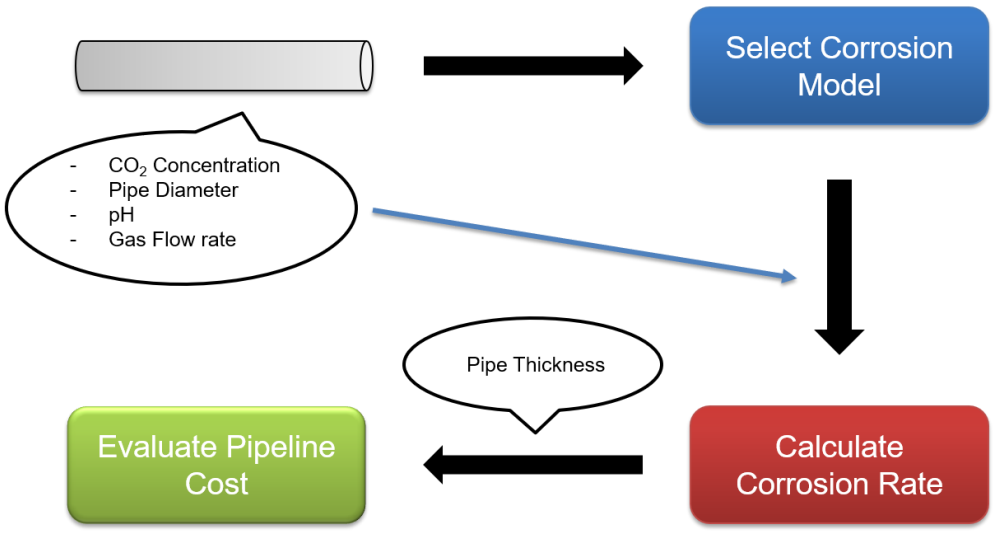

Figure 13: Work Flow for the Pipeline Cost Evaluation

For estimating the pipeline cost due to the corrosion. Figure shows how this part works. First, the CO_2 final concentration is determined from the simulations. Then the other variables can be determined such as pH and wall shear stress. Then after the corrosion model has been selected in this case, the NORSOK Model, the corrosion rate can be calculated for each case of CO_2 final concentration and therefore, the cost of the pipeline can be estimated by using the pipe thickness and length. To be more precise, the pipeline cost will be varied mainly because of the pipe thickness due to the CO_2 corrosion. The higher the CO_2 corrosion rate, the pipeline thickness will have and thereby, higher total pipeline cost. First, the larger pipeline thickness has to be calculated. It can be determined by the following step: First, the final concentration of CO_2 is obtained from the simulation. Next, the length of the pipeline is needed to be determine. However, the length of the pipe is also considered as a variable because as the length is higher, the cost for the pipeline materials are higher. Therefore, let L be the pipeline total length. The transmission line from the process to the LNG plants is assumed to be perfectly horizontal (neglecting for example, the bending in the pipelines or changes in heights). Then the pressure at the initial point after compression can be found by using Bernouli's Equation assuming the consumer's end pressure to be 70 bar. Then the corrosion rate can be determined and is resulted in the pipeline thickness. The Bernouli's equation is expressed as:

$$\frac{P_1}{\rho g} + \frac{u^2}{2g} + z_1 = \frac{P_2}{\rho g} + \frac{v^2}{2g} + z_2 + h_{loss} \tag{47}$$

Where P_2 in this case is the customer's end pressure which is 70 bar and the pressure P_1 is the pressure after the compression to the transmission line. Then the corrosion rate will be determine using the information in the previous sections and the partial pressure of CO_2 which is related to the total pressure. After that, the pipeline thickness can be obtained. From the

information given in section 2, the corrosion rate without the use of the corrosion inhibitor and the pipeline inside and outside diameters can be determined and shown in Table 14.

Table 14: Conclusion of Evaluating the Corrosion Rate and Pipe Diamters

CO_2 Final Concentration (mol%)	Corrosion Rate (mm/year)	Outside Diameter (m)	Inside Diameter (m)
1	6.8	0.902	0.794
1.5	8.8	0.926	0.797
2	11	0.927	0.797
2.5	12	0.950	0.800
3	14	0.963	0.802
3.5	15	0.985	0.804
4	16	0.100	0.807
4.5	18	1.032	0.811
5	19	1.044	0.813
5.5	20	1.056	0.815
6	22	1.079	0.818

From the information given in Table 14 , the relationship between the CO_2 corrosion rate which is expressed as mm/year and the CO_2 final concentration can be plotted and shown in Figure 14.

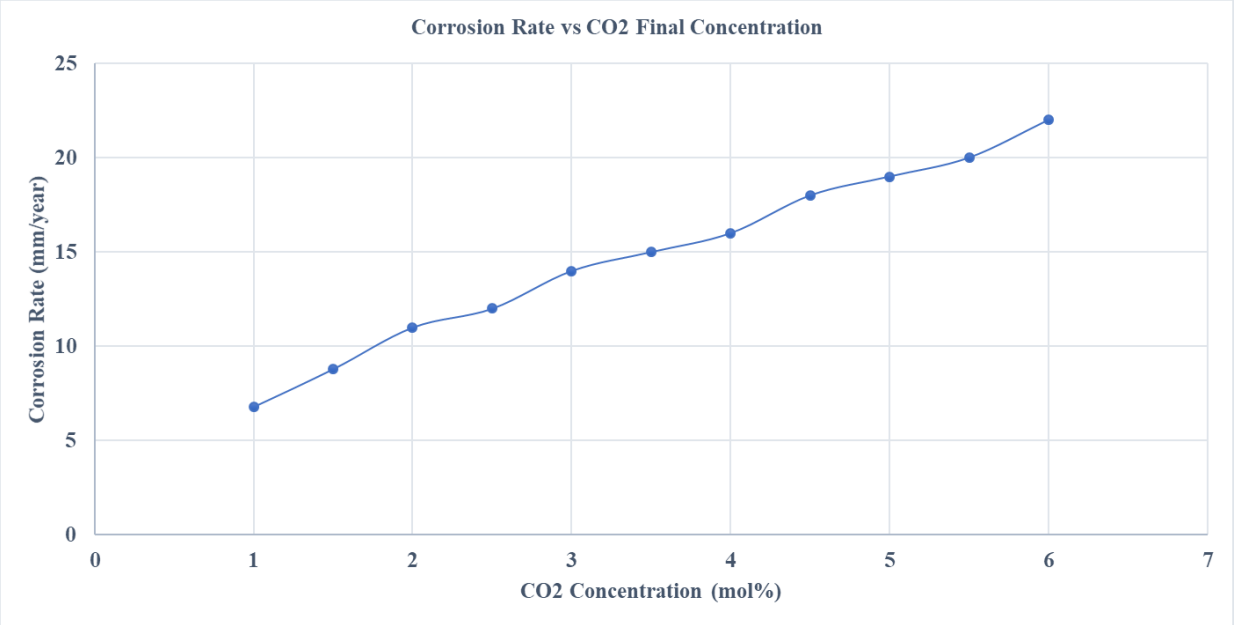

Figure 14: Relationship between the Corrosion Rate and the CO_2 Final Concentration

In Figure 14, as the CO_2 concentration is higher, the corrosion rate is higher as expected from the higher probability to form carbonic acid in pipelines. From this, at higher concentration, the pipeline thickness is needed to be thicker and therefore, the cost of the pipeline should be higher as well. The pipeline cost determination would be based on the corrosion rate given in the previous table.

As discussed in the section 3.5, the pipe standard must be

met to be able to construct a suitable pipe. Therefore, the standard thickness for the pipe is 19 mm. Therefore, the pipeline must have inhibitors to make the pipe meets the standards. Table 15 shows how much concentrated the inhibitors is needed to be in each concentration.

Table 15: Inhibitor Concentration for each CO_2 Concentration

CO_2 Final Concentration (mol%)	Corrosion Rate (mm/year)	Inhibitor Concentration (ppm)
1	6.8	9.00
1.5	8.8	9.20
2	11	9.60
2.5	12	9.80
3	14	9.83
3.5	15	9.88
4	16	9.90
4.5	18	9.95
5	19	10.00
5.5	20	10.20
6	22	10.70

From this data, the cost of the inhibitors can be estimated to be combined with the pipeline cost and operating cost in the next part.

The pipeline capital and operation cost were obtained by combining Knoope's and Wei's work [27, 28]. The calculation includes first, the capital cost of the pipeline which consists of the pipeline material, civil engineering cost, pipe installation cost, inhibitors and equipment cost, land acquisition cost, labor cost and miscellaneous cost. Then there is also indirect cost and other cost.

Operation and maintenance cost are also an important part of the evaluation. It includes pipeline labor, power, daily repairs, indirect cost and other expenses. All the cost combined can form a total capital cost and also the total operation cost per year of the whole transmission line. An example of the pipeline capital cost and operating cost for amine absorption at 100 km pipeline length and with the consideration of inhibitor can be summarized in Table 16. The total evaluation was done from the pipeline length of 10 km to 300 km because those ranges are the typical pipeline length from the customers' end to the plant both offshore and onshore.

Table 16: Pipeline Cost Summarization for Amine Absorption

CO_2 Final Concentration (mol%)	**Capital cost (Million USD)**	**Operating Cost (Million USD)**
1	117	3.74
1.5	141	4.18
2	167	4.68
2.5	179	4.92
3	204	5.39
3.5	217	5.63
4	230	5.89
4.5	256	6.38
5	270	6.64
5.5	283	6.90
6	311	7.42

Like amine absorption, the pipeline total cost for the physical absorption process by using selexol as solvent at 100 km pipeline length can also be summarized in Table 17,

Table 17: Pipeline cost Summarization for Physical Absorption

CO_2 Final Concentration (mol%)	**Capital cost (Million USD)**	**Operating Cost (Million USD)**
1	130	4.00
1.5	157	4.50
2	187	5.06
2.5	202	5.34
3	230	5.86
3.5	245	6.16
4	260	6.45
4.5	290	7.01
5	305	7.31
5.5	320	7.59
6	352	8.20

However, if the length of the pipeline changes, the pipeline capital cost and the operating cost will both change which would affect the economic comparison in the next chapter.

CHAPTER IV

ECONOMICS COMPARISON

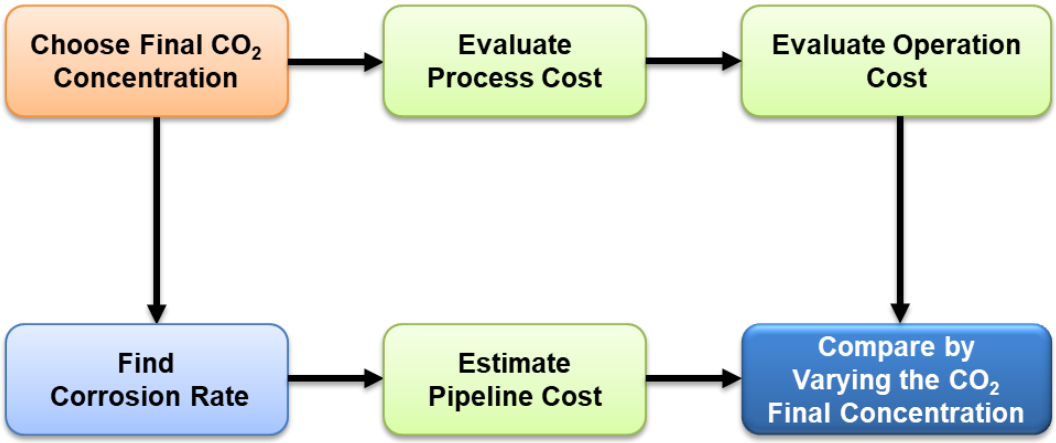

Figure 15: Economics Comparison Work Flow

Figure 15 shows how the comparison between the processes at each CO_2 concentration can be made. After choosing the final CO_2 concentration, the determination of the process cost which includes the operating cost and capital cost is done. Then the corrosion rate was obtained by the CO_2 concentration. The pipeline cost was also found. By comparing the process cost and the pipeline cost, the most suitable operating conditions for each process can be defined. Also, the best process for the CO_2 concentration can be selected regarding the results from the previous section. The economic factor that is used to select the suitable process is the internal rate of return (IRR). IRR is a very useful indicator to compare between different projects. It is independent of the project size unlike net present value (NPV) which would be larger as the project is bigger and it can also be compared directly to the interest rate [29]. The value of IRR in this work is evaluated by using Towler's book by assuming tax of 35%, a straight-line depreciation and an operating time of 15

years. The summarization of IRR calculations for amine absorption at 100 km length of pipeline can be shown in Table 18,

Table 18: IRR Value for each CO_2 Concentration for Amine Absorption process at 100 km Pipeline Length

CO_2 Final Concentration (mol%)	**IRR (year-%)**
1	32.03
1.5	33.71
2	32.97
2.5	33.51
3	31.70
3.5	31.82
4	31.40
4.5	29.60
5	25.66
5.5	24.93
6	23.51

As shown in Table 18, the maximum IRR for this specific case is 33.71 year-% at 1.5 mol% final CO_2 concentration. However, this is only the case for the pipeline length of 100 km. If there is any variation in the pipeline length, the suitable final CO_2 concentration will change as well due

to the change in the amount of pipeline material used and other expenses. Thus, in this project, determination of the IRR in the range between 10 km to 300 km with an interval of 10 km were to be considered. For example, at 50 km the IRR for every concentration is not the same as at 100 km and the optimal CO_2 concentration may not be at 1.5%. Therefore, from all the IRR in these ranges, the relationship between the pipeline length and the optimized CO_2 concentration can be obtained to give the optimized CO_2 concentration for each length of pipeline. For physical absorption, similar results can also be achieved.

As mentioned in the previous section, the difference of the pipeline length affects the IRR in each concentration on both processes. The plot between the optimal CO_2 concentration and the pipeline length can be shown in Figure 16 and Figure 17.

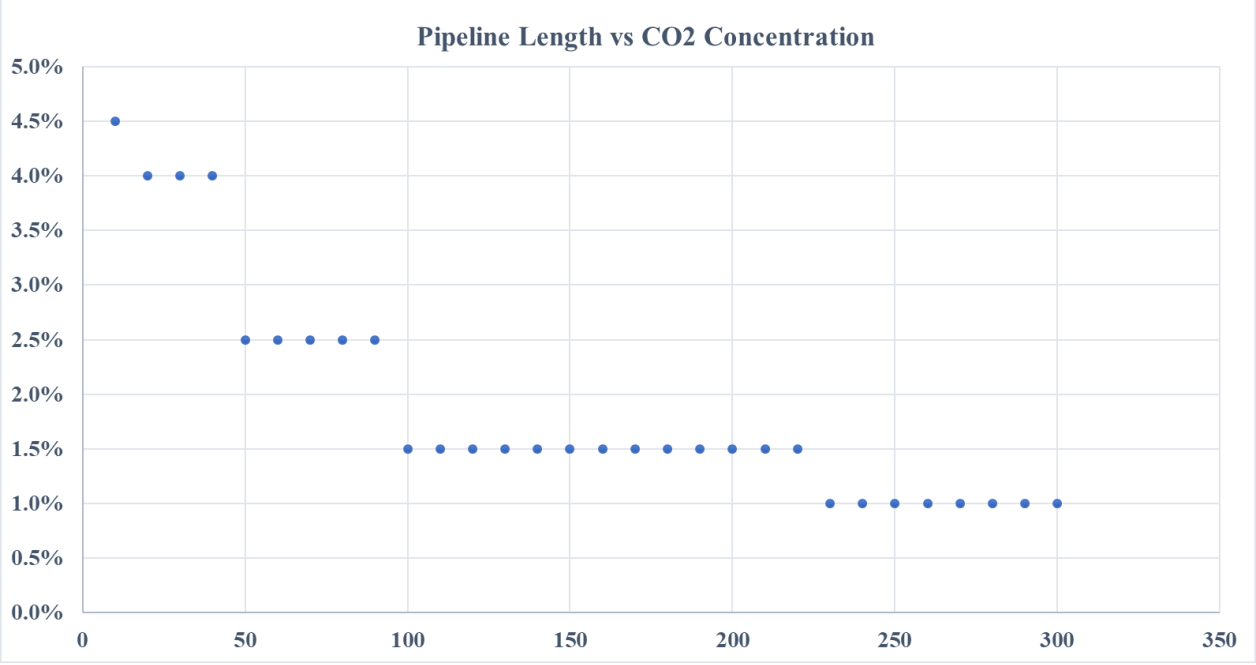

Figure 16: Relationship for Pipeline Length and CO_2 Concentration for Amine Absorption

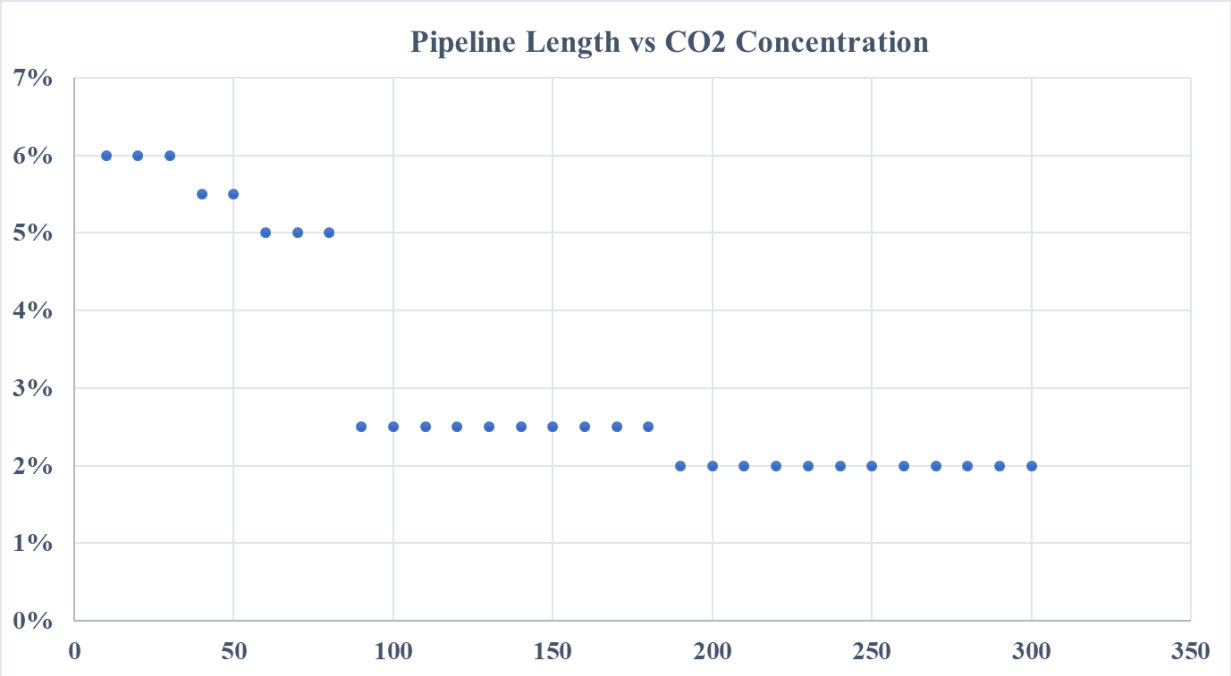

Figure 17: Relationship for Pipeline Length and CO2 Concentration for Physical Absorption

From Figure 16 which is the relationship created from the amine absorption process, the optimal CO_2 concentration of 4.5% is only at the pipeline length of 10 km. Then at 20 – 40 km, the optimal point is 4%. Similarly, the optimal point for the range of 50 – 90 km, 100 – 200 km and 220 – 300 km are 2.5%, 1.5% and 1% respectively. The same analysis can be done for the physical absorption by considering Figure 17 which the optimal point for the range of 10 – 30 km, 40 – 50 km, 60 – 80 km, 90 – 180 km and 190 – 300 km are 6%, 5.5%, 5%, 2.5% and 2% respectively. When considering the trend of the relationships, as the pipeline length is higher, the optimal point tends to run towards the lower CO_2 concentration. This is because at lower pipeline length, the impact of the operating cost dominates the effect of the pipeline cost which is low because of its' short length. On the other hand, at long distance, the pipeline cost from the

materials and others overcome the effect of the operating cost. Therefore, from the information obtained above, the behavior of the IRR and CO_2 concentration in each range of the pipelines for both processes are shown in Figure 18 to Figure 22,

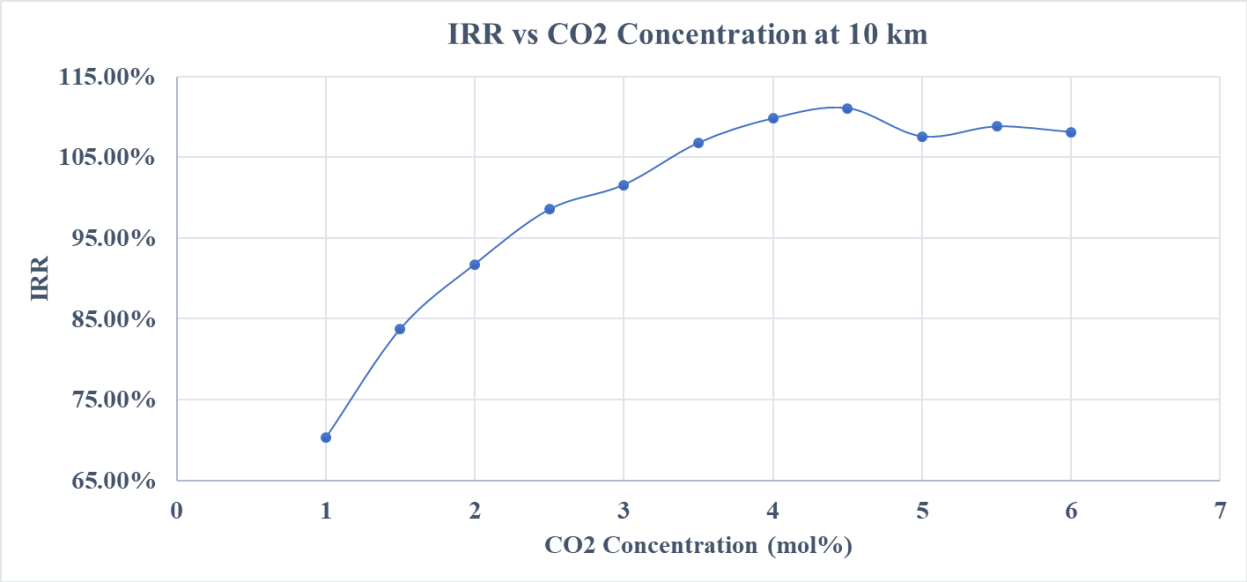

Figure 18: IRR vs CO_2 Concentration at 10 km (Amine Absorption)

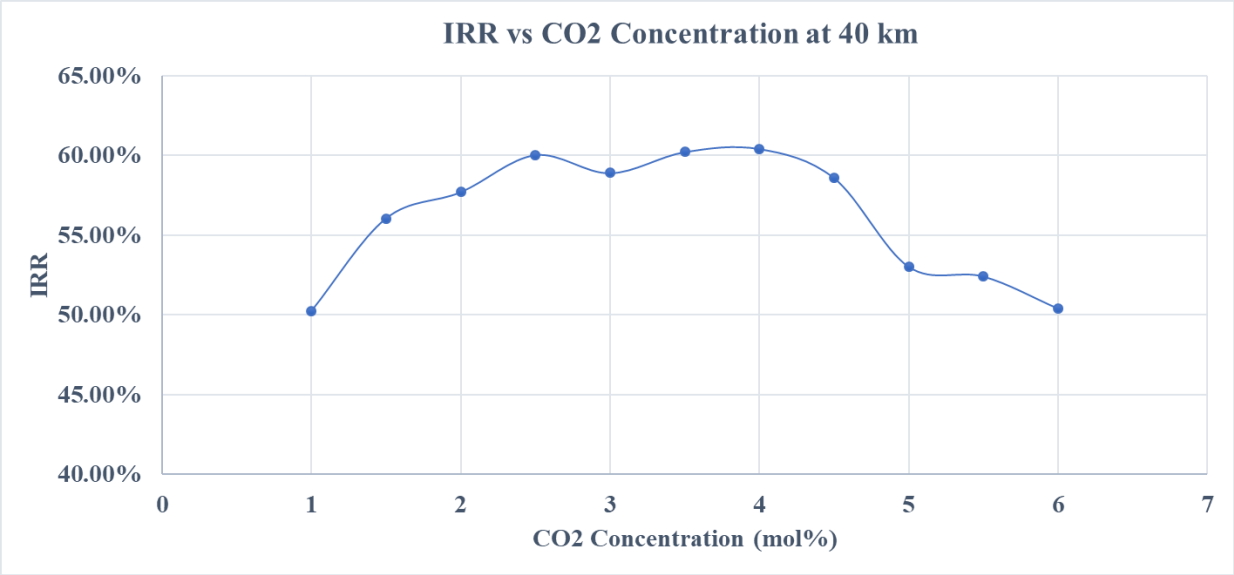

Figure 19: IRR vs CO2 Concentration at 40 km (Amine Absorption)

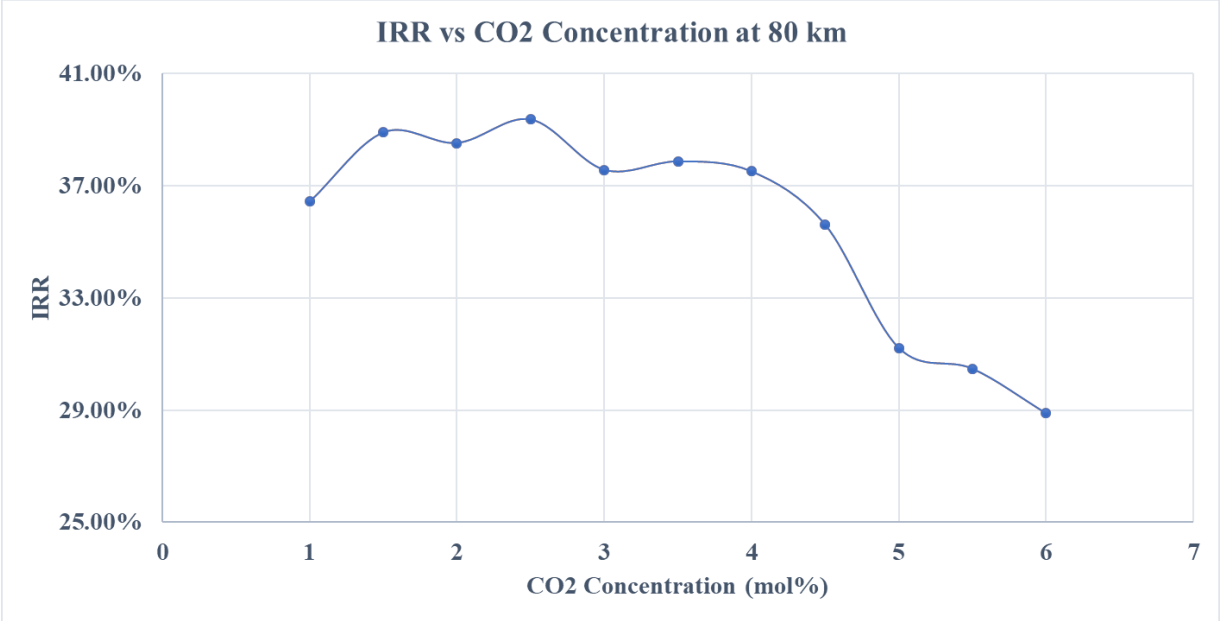

Figure 20: IRR vs CO2 Concentration at 80 km (Amine Absorption)

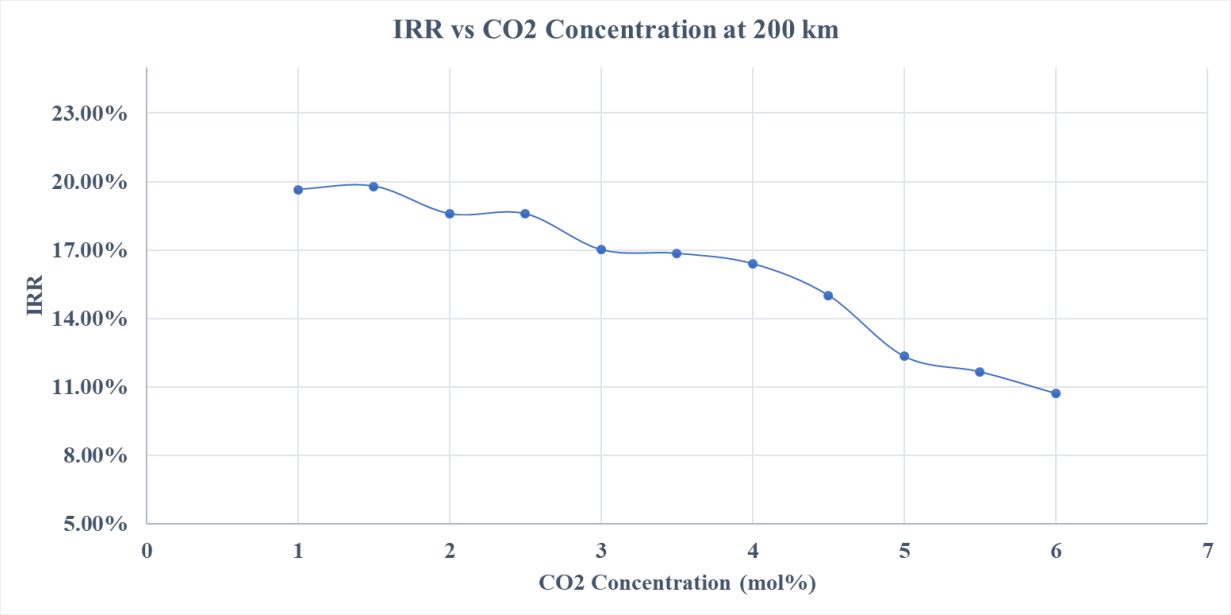

Figure 21: IRR vs CO2 Concentration at 200 km (Amine Absorption)

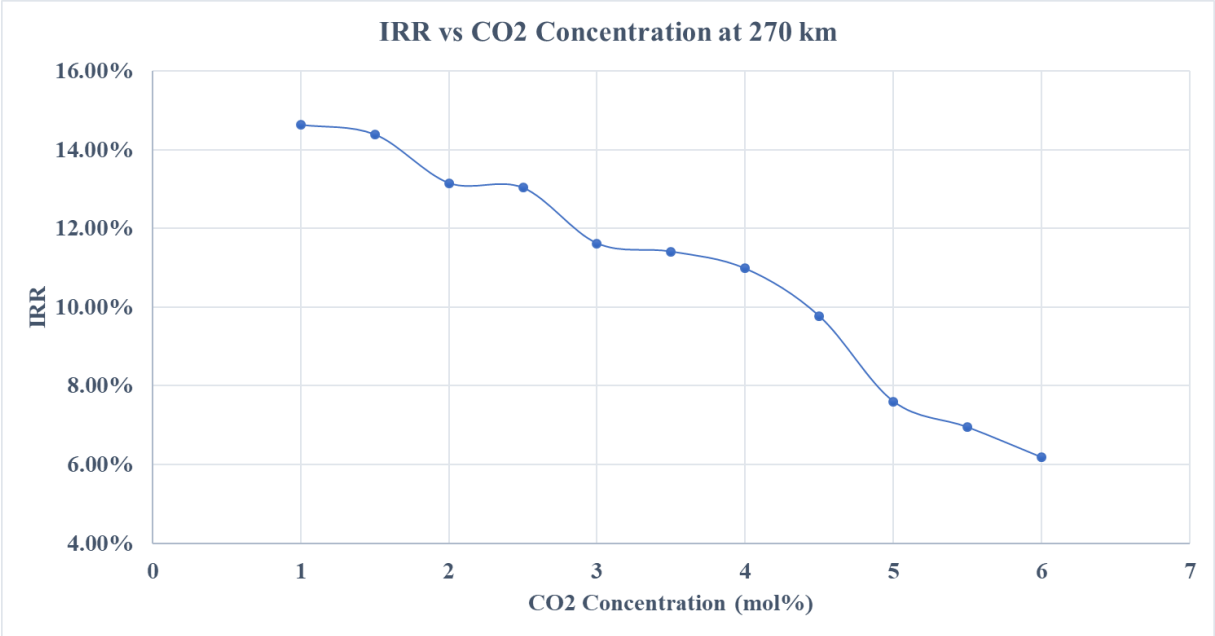

Figure 22: IRR vs CO2 Concentration at 270 km (Amine Absorption)

From all the behaviors above, there is an optimal point which gives the maximum IRR and CO_2 concentration. In addition, the relationships agree with the analysis that the optimal point goes towards the lower CO_2 concentration as the pipeline length is longer. However, the higher the length of the pipeline, the less the maximum IRR. Thus, in the longer range of the pipeline, the plant or process may not be good economically. Therefore, the relationship between the maximum IRR and the pipeline length is generated in the Figure 23.

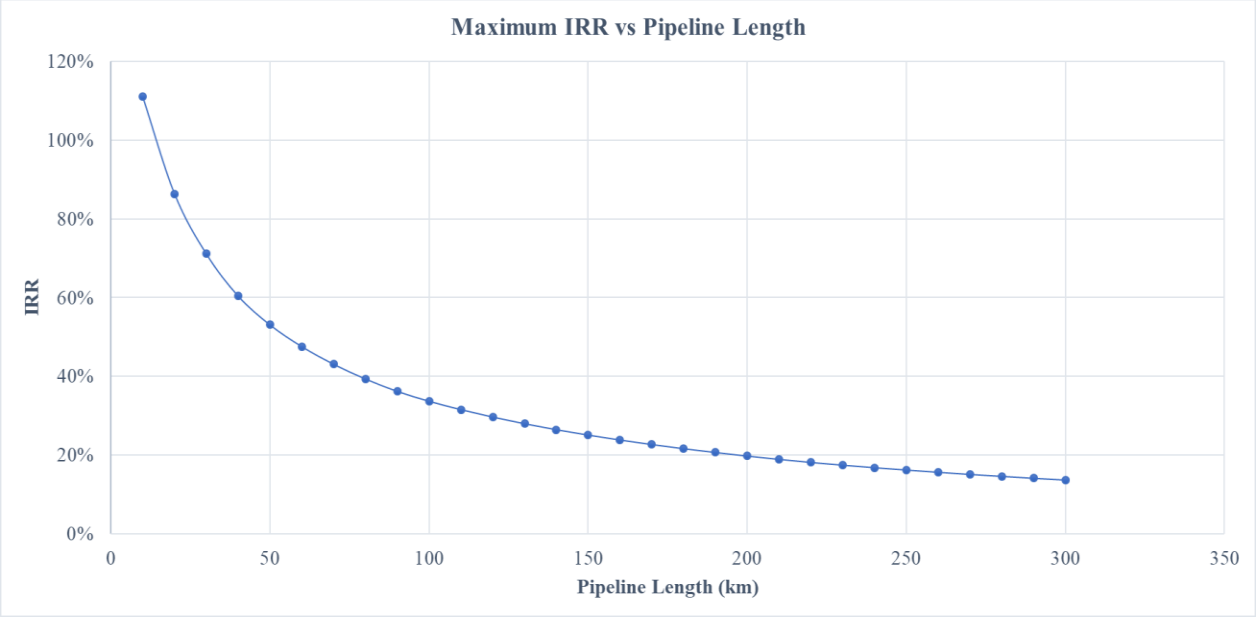

Figure 23: Maximum IRR for each Pipeline Length

The maximum IRR given in Figure 23 is the optimal point for each length of pipeline. For instance, at 150 km, the maximum IRR is 25.12 year-% at 1.5 mol% CO_2 final concentration. The plot shows that as the pipeline length is longer the IRR decreases. Moreover, the decreasing rate is higher as the pipeline length grows and finally, the rate becomes stable at about 200 km. In

addition, from this plot, the IRR value in the latter part of this relationship is relatively low compared to typical decent projects in the industries. Some is below 20 year-% which may not satisfy some project's economical goal. This project is an oil and gas project which have high risks so an IRR of 20 year-% is relatively low. Therefore, a conclusion can be made that at more than 180 km, the project might not be good economically. On the other hand, if the project increases the sales gas flow rate, the revenue will increase and result in a higher IRR which may reach the objective of the project.

The summarization of the IRR in each range of pipeline can also be conducted for the physical absorption case in Figure 24 to Figure 28.

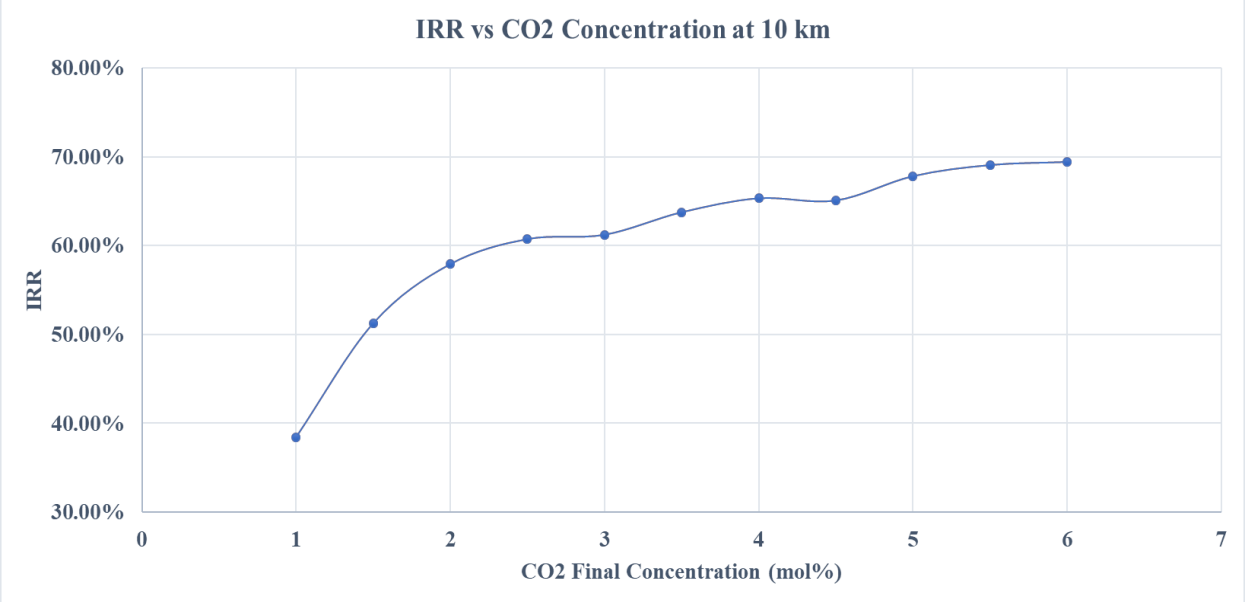

Figure 24: IRR vs CO2 Concentration at 10 km (Physical Absorption)

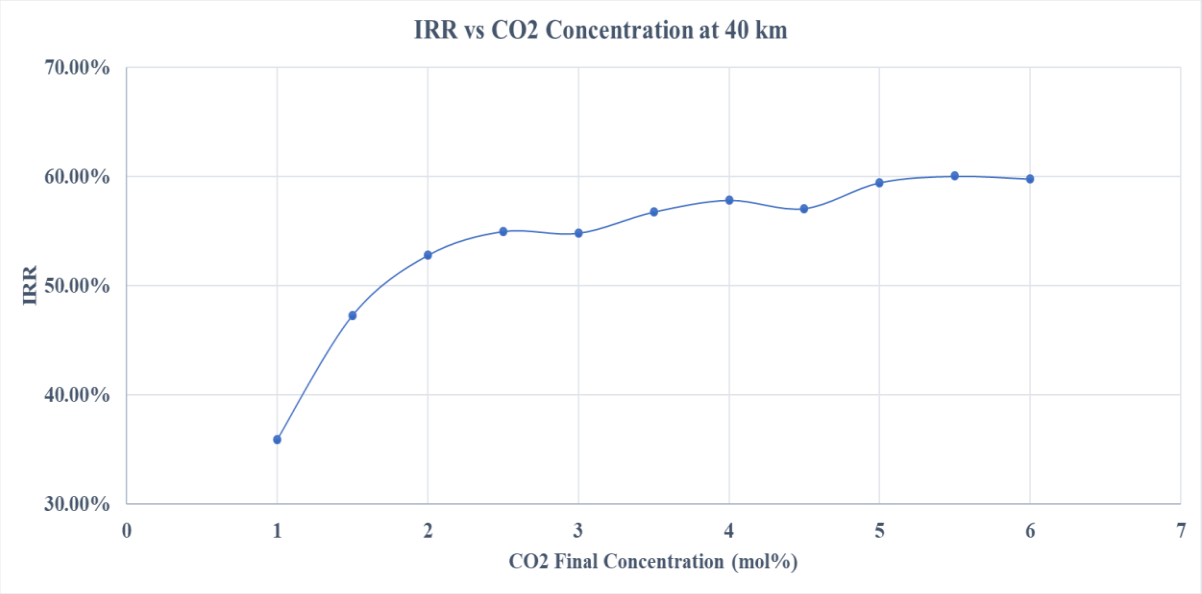

Figure 25: IRR vs CO2 Concentration at 40 km (Physical Absorption)

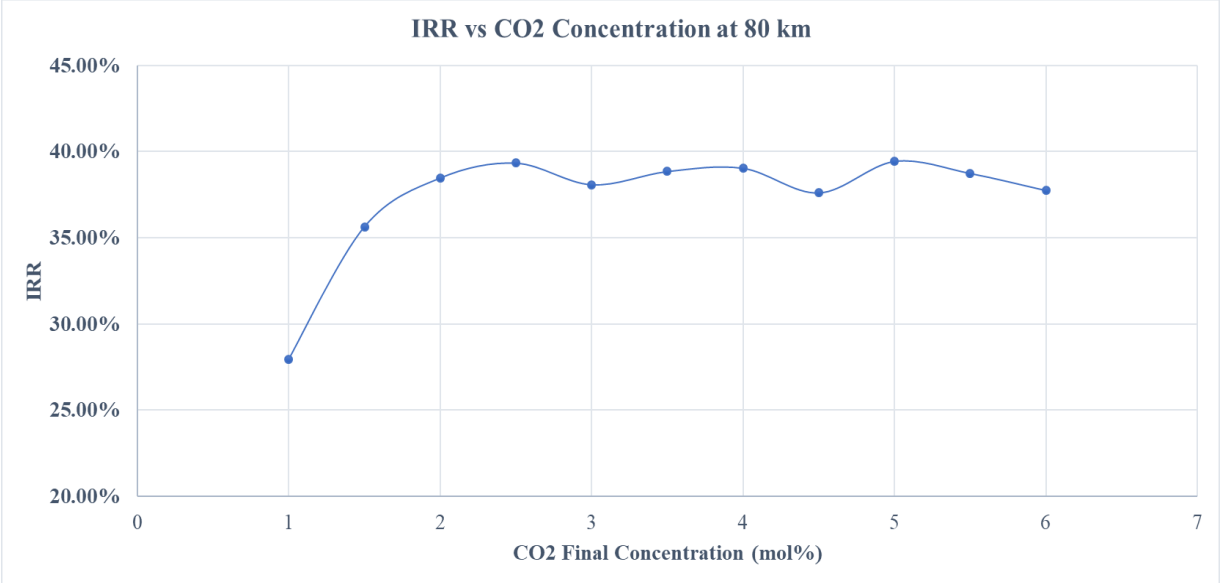

Figure 26: IRR vs CO2 Concentration at 80 km (Physical Absorption)

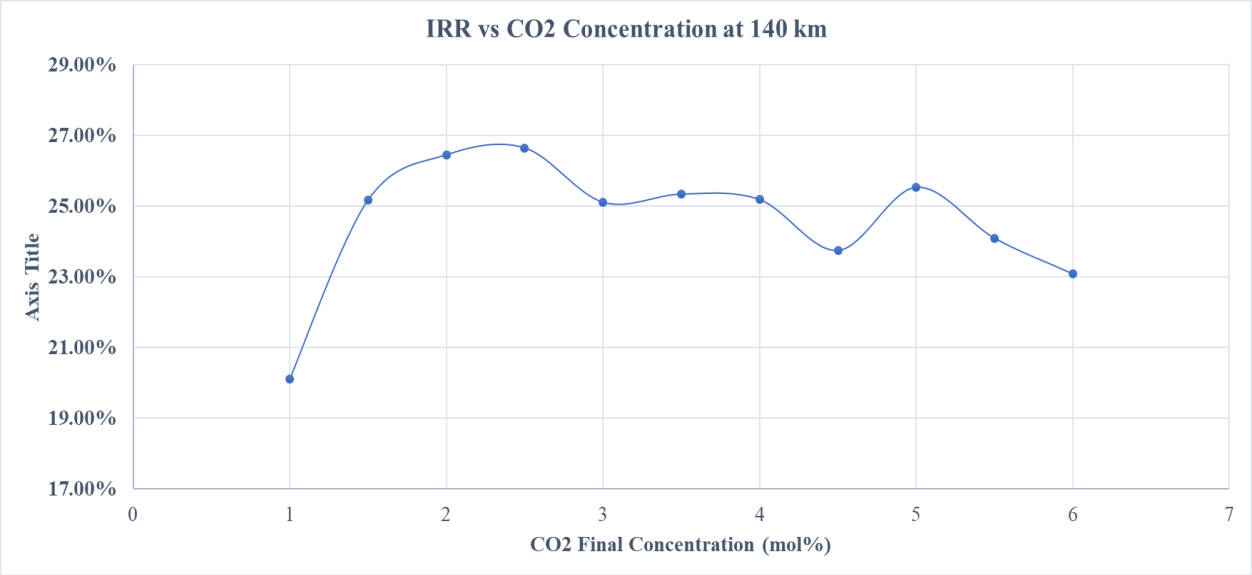

Figure 27: IRR vs CO2 Concentration at 140 km (Physical Absorption)

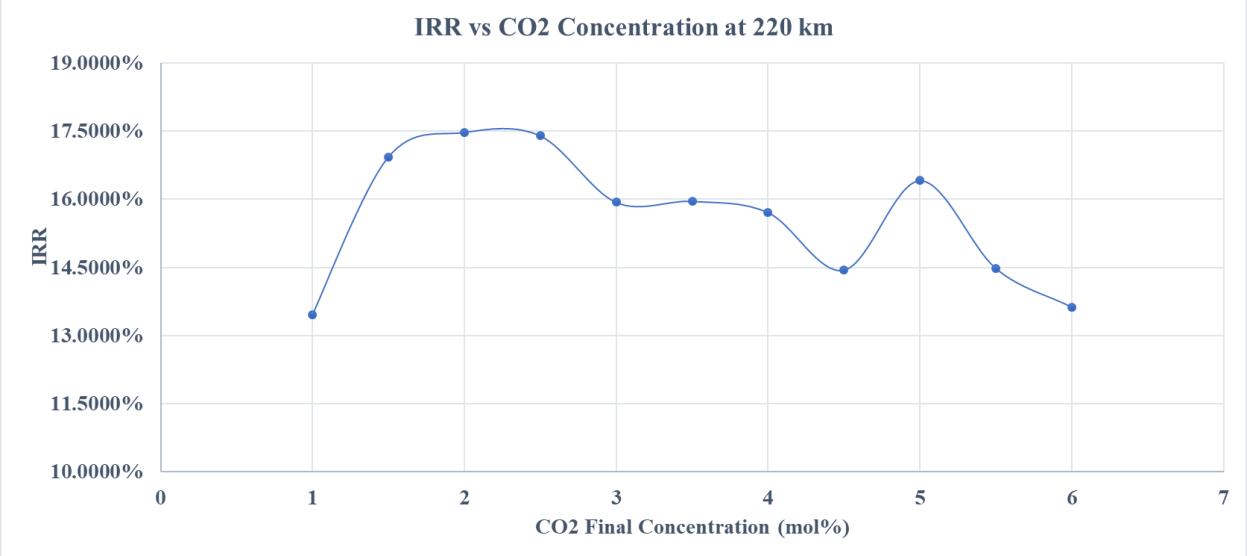

Figure 28: IRR vs CO2 Concentration at 220 km (Physical Absorption)

The results are similar to the amine absorption case, there is an optimal point for each range of the CO2 concentration and also tends to go towards the lower CO_2 concentration as the pipeline

length is larger. Moreover, the relationship between the maximum IRR and the length of the pipeline can also be plotted in Figure 29. However, in this physical absorption part, even if the pipeline length is even longer than 300 km, the optimal CO_2 concentration does not goes below 2%mol this might be because of the cost of the physical absorption at 1.5%mol and 1%mol are relatively high comparing to the higher concentration of the CO_2

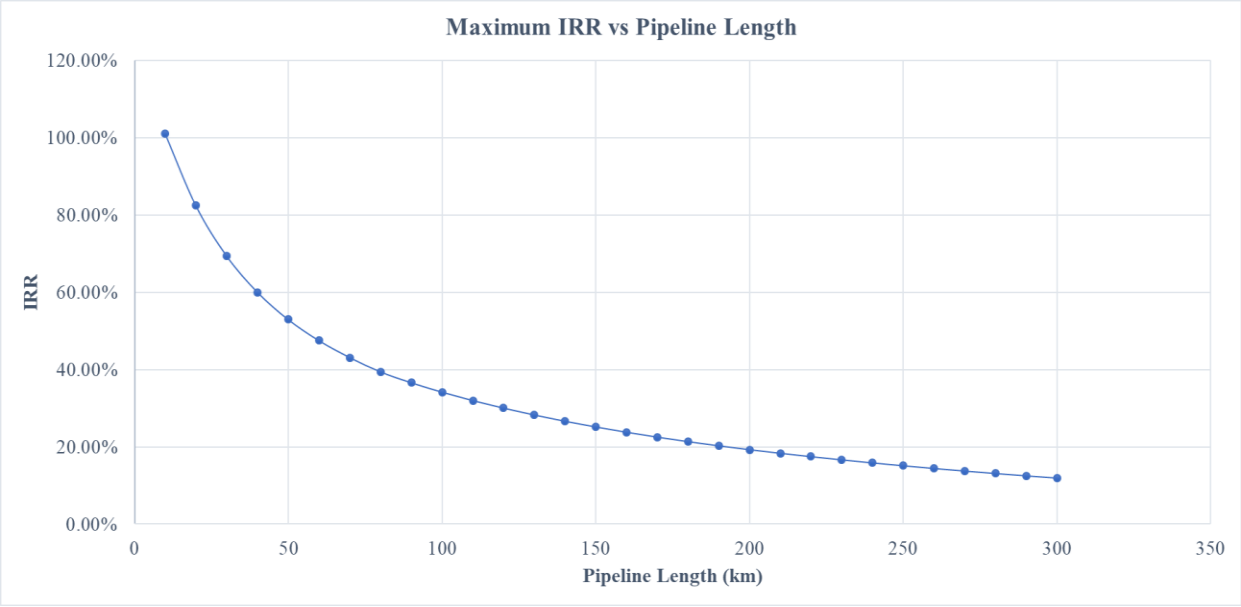

Figure 29: Maximum IRR at each Pipeline Length for Physical Absorption

From Figure 29, a conclusion can also be made if the IRR is less than 20 year-%, it is considered as a low value that at more than 200 km length of pipeline, physical absorption may not be a good choice and also, if the sales gas flow is higher, then the IRR value can be improved as well.

The last objective of this thesis is to compare the amine absorption process and the physical process to see the optimal point for each pipeline length and CO_2 concentration. Therefore, Figure 23 and Figure 29 can be combined to perform a comparison between the processes to select the suitable process for different pipeline lengths. The relationship is shown in Figure 30.

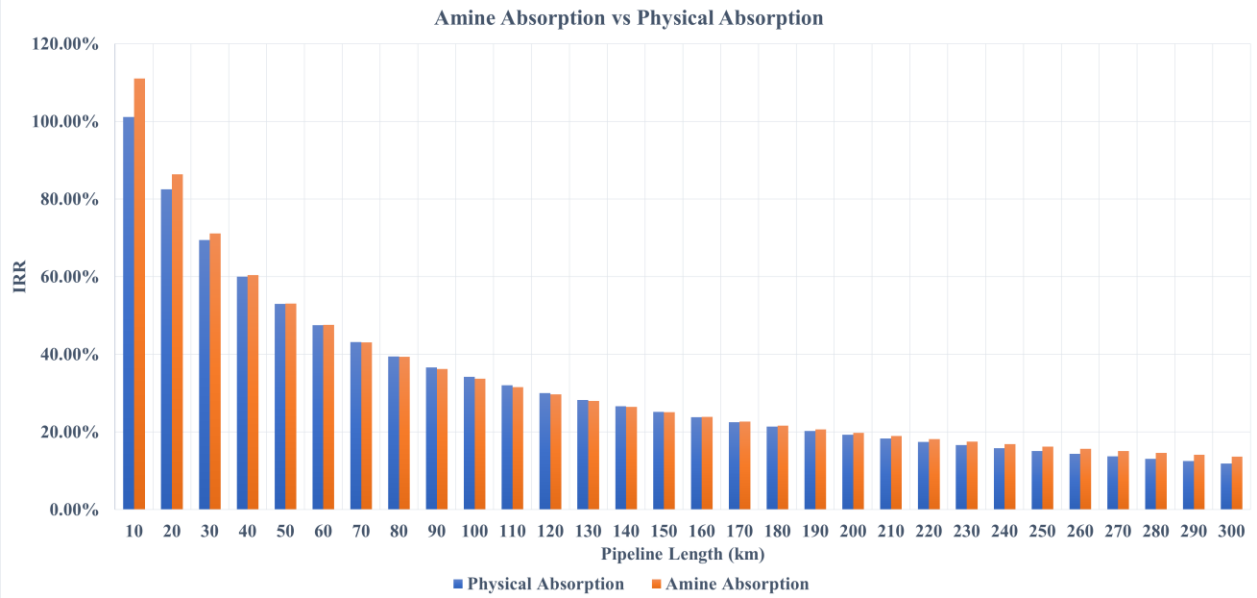

Figure 30: Maximum IRR Comparison for Both Processes at each Pipeline Length

From Figure 30, the IRR for amine absorption in the shorter range between 10 to 60 km is higher than the IRR for physical absorption. Then after 70 km until 150 km the IRR for physical absorption is higher. Then the amine absorption is higher than the physical absorption process from 160 km point onwards. Therefore, the summarization of the results and the optimal process and concentration for each pipeline length are carried out in the next table.

Table 19: Summarization of the Optimal Point and Process in Different Pipeline Length

Pipeline length (km)	Optimal Process	IRR (year-%)	CO_2 Concentration (mol%)
10	Amine Absorption	111	4.5
20	Amine Absorption	86	4.0
30	Amine Absorption	71	4.0
40	Amine Absorption	60	4.0
50	Amine Absorption	53	2.5
60	Physical Absorption	47	5.0
70	Physical Absorption	43	5.0
80	Physical Absorption	39	5.0
90	Physical Absorption	37	2.5
100	Physical Absorption	34	2.5
110	Physical Absorption	32	2.5
120	Physical Absorption	30	2.5
130	Physical Absorption	28	2.5
140	Physical Absorption	27	2.5
150	Physical Absorption	25	2.5
160	Amine Absorption	24	1.5
170	Amine Absorption	23	1.5
180	Amine Absorption	22	1.5

Table 19 Continued

Pipeline length (km)	Optimal Process	IRR (year-%)	CO_2 Concentration (mol%)
190	Amine Absorption	21	1.5
200	Amine Absorption	20	1.5
210	Amine Absorption	19	1.5
220	Amine Absorption	18	1.5
230	Amine Absorption	17	1.5
240	Amine Absorption	17	1.0
250	Amine Absorption	16	1.0
260	Amine Absorption	16	1.0
270	Amine Absorption	15	1.0
280	Amine Absorption	15	1.0
290	Amine Absorption	14	1.0
300	Amine Absorption	14	1.0

Table 19 gives the optimal condition for each pipeline length. Nevertheless, there are some ranges of pipeline length which the IRR is considered as relatively high. For example, at 10 km, the optimal IRR is 111 year-% using amine absorption and operates at 4.5% mol. The reason for this extremely high IRR is because, the possibility of finding a natural gas site which gives the gas flow of more the 200 MMSCFD at short distance from the shore or from natural gas plant is relatively low. Therefore, if there is a drilling site that is able to achieve that flow, it is possible to have a really high return rate from the project. In addition, this work is based on only the maximum

IRR in each pipeline length. Some of the ranges as shown in Figure 30, the IRR are relatively close. However, this research is based on many assumptions so that maybe in that range, the other process might be better. If more information is known, the results can be more accurate.

CHAPTER V

CONCLUSIONS, RECOMMENDATIONS AND FUTURE WORK

5.1 Conclusions

In this work, the processes that chosen were amine absorption and physical absorption which can reduce the CO_2 in natural gas to a required specification were simulated using Aspen Hysys V8.8. The simulation was performed by varying the CO_2 final concentration in the sales gas stream from 1% to 6% mol. Then the cost of the process was evaluated by combining Towler's methodology and data from the simulation. Results indicated that as the final concentration of CO_2 lowered, the cost of the process would be higher for both of the process types. The pipeline cost is affected by the corrosion from the CO_2. Therefore, the corrosion of CO_2 in pipelines was studied and the rate of corrosion was obtained by using NORSOK model. This study concluded that the more CO_2 is in the gas stream, the corrosion rate would be higher in the transmission lines. After the corrosion rate was calculated, the pipeline total cost was also evaluated as well. The pipeline cost is higher as the corrosion rate is higher. Thereby, reducing the CO_2 concentration can help minimize the pipeline cost. Moreover, the pipeline length also caused the differences in the IRR values. Thereby, the pipeline distance was also considered as one of the variables by varying the pipeline length between 10 – 300 km. The decision of choosing the optimal point and process was done by combining all the cost and determined the IRR of the project for both processes.

The goal of this research is to compare the processes and select the suitable process for the operations. Economics results showed that there is a range of the pipeline length which amine absorption gave a better IRR than physical absorption. On the other hand, in some other ranges, the physical absorption gave a more decent result and as the pipeline length is higher, both processes optimal concentration tended to go towards lower CO_2 concentration. Therefore, the

process selection can be made according to the results, if the results are accurate. However, due to many uncertainties in the cost evaluation, the results need more validation. In some ranges of the pipeline length, the maximum IRR of the process is differed only by a little. Thus, the process with the higher IRR in that range may not really be better.

In conclusion, this project gives a working process that can be used to select the suitable process for certain natural gas composition and the distance from the production platform to the customers' end. Most companies and investors tend to operate plants and pipeline according to the maximum specifications which in this project shows that it might not always be the best case.

5.2 Recommendations

In this work, the freezing in pipelines were not considered at all and assumed to have no effects on the pipeline and process equipment. However, in practical, it might affect the process in some ways. Thus, to make the work more accurate, the suggestion is to find a way to involve the effect of CO_2 freezing or hydrate formation to the research. Moreover, some materials and inhibitor cost used in this project was obtained from old sources. Therefore, more precise cost for these materials can make the work more reliable. Finally, a sensitivity analysis by varying the cost of some materials or others can also lessen the uncertainties.

5.3 Future Work

As already mentioned in the section 5.2, the future work can include: the consideration of CO_2 freezing and hydrate formation in pipelines and process equipment, the cost of the materials and other during the process. Moreover, other acid gas and the effect of the solvents such as amine itself in pipelines can also be considered to make the work perfect.

NOMENCLATURE

CR_t	Corrosion rate at temperature t (mm/year)
K_t	Constant for temperature t used in the corrosion rate calculations
K_i	Equilibrium constant used in pH and other calculations
K_w	Equilibrium constant for water
K_{Sp}	Equilibrium constant for iron carbonate
S	Wall Shear Stress (Pa)
f_{CO2}	fugacity of CO_2 (bar)
f(pH)	pH factor
ρ_m	Mixed density (kg/m^3)
ρ_L	Liquid density (kg/m^3)
ρ_g	Gas density (kg/m^3)
ρ_w	Water density (kg/m^3)
ρ_0	Oil density (kg/m^3)
ϕ	Watercut
ϕ_C	Watercut at inversion point
λ	Liquid fraction
u_m	Mixed velocity (m/s)
u_L^s	Superficial velocity of liquid (m/s)
u_G^s	Superficial velocity of gas (m/s)
Q_L	Volumetric flowrate of liquid (Sm^3/day)

Q_G	Volumetric flowrate of gas (Sm^3/day)
A	Area (m^2)
Z	Compressibility of gas
P	Pressure (bar)
T	Temperature
T_f	Temperature in Fahrenheit
T_{std}	Temperature given in Kelvin at standard conditions
μ_m	Mixed viscosity (Ns/m^2)
μ_L	Liquid viscosity (Ns/m^2)
μ_G	Gas viscosity (Ns/m^2)
μ_0	Oil viscosity (Ns/m^2)
μ_{relmax}	Maximum relative viscosity (Ns/m^2)

REFERENCES

1. Strategies, G., *The Outlook for LNG in 2016.* 2016.
2. (IGU), I.G.U., *2016 World LNG Report*. 2016.
3. Ebenezer, S.A. and J. Gudmunsson, *Removal of carbon dioxide from natural gas for LNG production.* Semester project work, 2005.
4. Figueroa, J.D., et al., *Advances in CO 2 capture technology—the US Department of Energy's Carbon Sequestration Program.* International journal of greenhouse gas control, 2008. **2**(1): p. 9-20.
5. Herzog, H., J. Meldon, and A. Hatton, *Advanced post-combustion CO2 capture.* Clean Air Task Force, 2009. **439**.
6. Zahid, U., et al., *Simulation and parametric analysis of CO2 capture from natural gas using diglycolamine.* International Journal of Greenhouse Gas Control, 2017. **57**: p. 42-51.
7. Shimekit, B. and H. Mukhtar, *Natural gas purification technologies-major advances for CO2 separation and future directions*, in *Advances in Natural Gas Technology*. 2012, InTech.
8. Kohl, A.L. and R. Nielsen, *Gas purification*. 1997: Elsevier.
9. Ritter, J. and A. Ebner, *Carbon dioxide separation technology: R&D needs for the chemical and petrochemical industries.* Chemical Industry Vision, 2007. **2020**: p. 287-295.
10. Kovvali, A.S. and K.K. Sirkar, *Carbon dioxide separation with novel solvents as liquid membranes.* Industrial & engineering chemistry research, 2002. **41**(9): p. 2287-2295.
11. Meyers, R.A., *Encyclopedia of physical science and technology*. 2002: academic.

12. Berstad, D., P. Nekså, and R. Anantharaman, *Low-temperature CO2 removal from natural gas.* Energy Procedia, 2012. **26**: p. 41-48.

13. Yang, J. and D. Kim, *Maximized Values of LNG Specifications in the LNG Industry: Producer and Buyer Perspectives.*

14. *Natural Gas Weekly Update*. 2018 September 26, 2018 [cited 2018 10/3]; Available from: https://www.eia.gov/naturalgas/weekly/.

15. Tsunatu, D., I. Mohammed-Dabo, and S. Waziri, *Technical Evaluation of Selexol-Based CO2 Capture Process for a Cement Plant.* Br. J. Environ. Clim. Change, 2015. **5**(1): p. 52-63.

16. Perez, T.E., *Corrosion in the oil and gas industry: an increasing challenge for materials.* Jom, 2013. **65**(8): p. 1033-1042.

17. Abbas, M.H., *Modelling CO2 corrosion of pipeline steels.* 2016.

18. De Waard, C., U. Lotz, and D. Milliams, *Predictive model for CO2 corrosion engineering in wet natural gas pipelines.* Corrosion, 1991. **47**(12): p. 976-985.

19. Nyborg, R., *Guidelines for prediction of CO2 corrosion in oil and gas production systems*. 2009: Institute for Energy Technology.

20. Nyborg, R. and A. Dugstad, *Reliability and limitations of corrosion prediction tools for oil and gas pipelines.* Eurocorr/2004 (Nice: CEFRACOR, 2004), 2004.

21. Gartland, P.O., I. Ovstetun, and R. Johnsen, *Application of internal corrosion modeling in the risk assessment of pipelines.* CORROSION 2003, 2003.

22. Nyborg, R. *Overview of CO2 corrosion models for wells and pipelines*. in *CORROSION 2002*. 2002. Nace International.

23. NORSOK, M., *506 NORSOK Standard M-506: CO2 Corrosion Rate Calculation Model*. Standards Norway, Lysaker, Norway, 2005.

24. *Pipes - Nominal Wall Thickness*. [cited 2018 4 October]; Available from: https://www.engineeringtoolbox.com/nominal-wall-thickness-pipe-d_1337.html.

25. Askari, M., et al., *Film former corrosion inhibitors for oil and gas pipelines-A technical review*. Journal of Natural Gas Science and Engineering, 2018.

26. Jovancicevic, V., et al. *CO2 corrosion inhibition by sulfur-containing organic compounds*. in *CORROSION 2000*. 2000. NACE International.

27. Knoope, M., et al., *Improved cost models for optimizing CO2 pipeline configuration for point-to-point pipelines and simple networks.* International Journal of Greenhouse Gas Control, 2014. **22**: p. 25-46.

28. Wei, N., et al., *Budget-type techno-economic model for onshore CO2 pipeline transportation in China.* International Journal of Greenhouse Gas Control, 2016. **51**: p. 176-192.

29. Towler, G. and R.K. Sinnott, *Chemical engineering design: principles, practice and economics of plant and process design*. 2012: Elsevier.

APPENDIX A

PROCESS SIMULATION FIGURES FROM ASPEN HYSYS

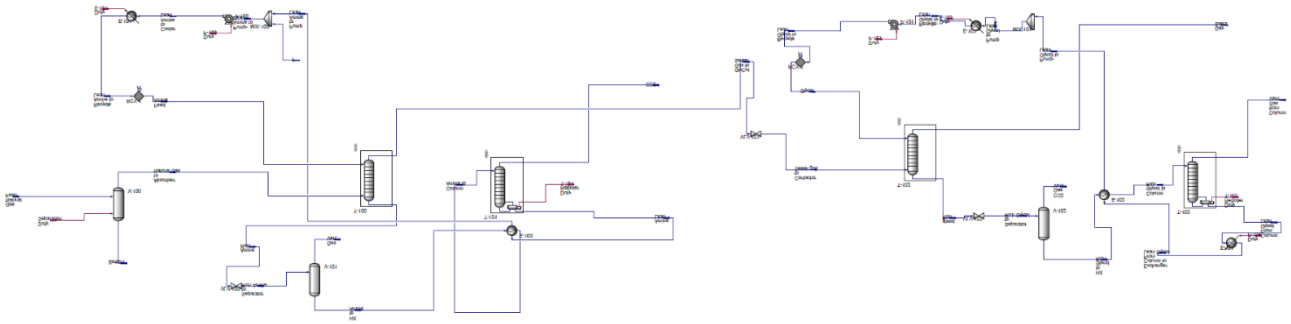

Figure 32: Amine Absorption Simulation from Aspen Hysys

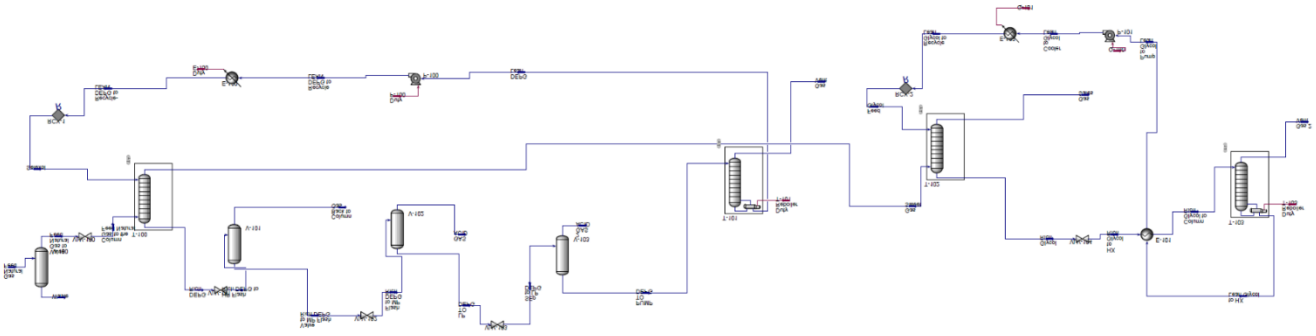

Figure 32: Physical Absorption Simulation from Aspen Hysys

APPENDIX B

IRR RESULTS

Table 20: IRR Results from 10 - 150 km for Amine Absorption

	10	20	30	40	50	60	70	80	90	100	110	120	130	140	150
IRR (yr-%)	108.11%	78.412%	61.39%	50.37%	42.64%	36.89%	32.44%	28.88%	25.96%	23.51%	21.42%	19.61%	18.03%	16.63%	15.39%
	108.80%	80.247%	63.45%	52.39%	44.55%	38.69%	34.13%	30.47%	27.46%	24.93%	22.77%	20.90%	19.26%	17.81%	16.52%
	107.57%	80.218%	63.87%	53.00%	45.25%	39.42%	34.87%	31.21%	28.20%	25.66%	23.49%	21.62%	19.97%	18.52%	17.22%
	111.07%	85.645%	69.61%	58.58%	50.54%	44.40%	39.55%	35.62%	32.36%	29.60%	27.24%	25.19%	23.39%	21.80%	20.37%
	109.81%	86.381%	71.13%	60.41%	52.48%	46.36%	41.49%	37.51%	34.20%	31.40%	28.98%	26.88%	25.04%	23.40%	21.93%
	106.78%	84.969%	70.51%	60.22%	52.53%	46.56%	41.79%	37.87%	34.60%	31.82%	29.42%	27.33%	25.49%	23.86%	22.39%
	101.58%	81.862%	68.52%	58.89%	51.62%	45.93%	41.34%	37.57%	34.40%	31.70%	29.36%	27.32%	25.52%	23.91%	22.47%
	98.54%	81.203%	69.04%	60.03%	53.09%	47.58%	43.10%	39.37%	36.21%	33.51%	31.16%	29.10%	27.27%	25.64%	24.18%
	91.76%	76.678%	65.85%	57.69%	51.33%	46.23%	42.04%	38.53%	35.55%	32.97%	30.73%	28.76%	27.00%	25.43%	24.02%
	83.75%	71.889%	62.98%	56.05%	50.49%	45.94%	42.13%	38.91%	36.13%	33.71%	31.58%	29.70%	28.01%	26.49%	25.12%
	70.26%	61.980%	55.47%	50.21%	45.87%	42.23%	39.12%	36.44%	34.09%	32.03%	30.19%	28.55%	27.06%	25.72%	24.49%

Table 21: IRR Results from 160 - 300 km for Amine Absorption

Length (km)	160	170	180	190	200	210	220	230	240	250	260	270	280	290	300
IRR (yr-%)	14.27%	13.25%	12.33%	11.49%	10.71%	9.99%	9.33%	8.71%	8.14%	7.60%	7.10%	6.63%	6.18%	5.76%	5.36%
	15.35%	14.30%	13.34%	12.47%	11.66%	10.91%	10.22%	9.58%	8.99%	8.43%	7.90%	7.41%	6.95%	6.51%	6.09%
	16.05%	14.99%	14.03%	13.15%	12.34%	11.59%	10.89%	10.25%	9.65%	9.09%	8.56%	8.07%	7.60%	7.16%	6.74%
	19.09%	17.93%	16.87%	15.90%	15.00%	14.18%	13.41%	12.70%	12.04%	11.42%	10.84%	10.29%	9.77%	9.28%	8.82%
	20.61%	19.41%	18.32%	17.32%	16.39%	15.54%	14.75%	14.01%	13.33%	12.69%	12.08%	11.51%	10.98%	10.47%	9.99%
	21.07%	19.87%	18.78%	17.77%	16.85%	15.99%	15.20%	14.46%	13.77%	13.13%	12.52%	11.95%	11.41%	10.90%	10.42%
	21.17%	19.99%	18.91%	17.92%	17.01%	16.13%	15.37%	14.64%	13.96%	13.32%	12.72%	12.15%	11.62%	11.11%	10.63%
	22.85%	21.64%	20.54%	19.52%	18.58%	17.71%	16.90%	16.15%	15.45%	14.79%	14.17%	13.58%	13.03%	12.51%	12.01%
	22.73%	21.56%	20.48%	19.50%	18.58%	17.73%	16.93%	16.21%	15.52%	14.88%	14.27%	13.69%	13.15%	12.64%	12.15%
	23.87%	22.72%	21.67%	20.69%	19.79%	18.95%	18.17%	17.43%	16.75%	16.11%	15.50%	14.93%	14.38%	13.87%	13.38%
	23.36%	22.33%	21.37%	20.48%	19.65%	18.88%	18.16%	17.48%	16.85%	16.24%	15.68%	15.14%	14.63%	14.15%	13.68%

Table 22 : IRR Results from 10 - 150 km for Physical Absorption

Length (km)	10	20	30	40	50	60	70	80	90	100	110	120	130	140	150
IRR (yr-%)	101.11%	82.47%	69.42%	59.79%	52.38%	46.50%	41.72%	37.74%	34.38%	31.49%	28.99%	26.78%	24.83%	23.08%	21.51%
	97.65%	81.05%	69.08%	60.04%	52.98%	47.31%	42.64%	38.73%	35.41%	32.54%	30.03%	27.82%	25.86%	24.09%	22.50%
	93.94%	78.83%	67.82%	59.44%	52.85%	47.53%	43.13%	39.44%	36.29%	33.57%	31.19%	29.08%	27.21%	25.53%	24.02%
	89.56%	75.50%	65.08%	57.07%	50.71%	45.54%	41.24%	37.61%	34.49%	31.79%	29.42%	27.31%	25.44%	23.75%	22.21%
	87.46%	74.89%	65.34%	57.83%	51.78%	46.79%	42.60%	39.04%	35.96%	33.27%	30.90%	28.79%	26.89%	25.19%	23.63%
	83.98%	72.57%	63.76%	56.75%	51.04%	46.29%	42.28%	38.85%	35.87%	33.25%	30.94%	28.88%	27.02%	25.34%	23.81%
	79.32%	69.19%	61.23%	54.81%	49.53%	45.10%	41.33%	38.08%	35.24%	32.75%	30.52%	28.53%	26.74%	25.11%	23.62%
	76.39%	67.73%	60.74%	54.97%	50.13%	46.00%	42.44%	39.34%	36.61%	34.18%	32.00%	30.04%	28.27%	26.65%	25.16%
	71.52%	64.06%	57.92%	52.77%	48.40%	44.63%	41.35%	38.47%	35.91%	33.63%	31.57%	29.70%	28.01%	26.45%	25.02%
	61.31%	55.87%	51.24%	47.26%	43.80%	40.75%	38.05%	35.63%	33.46%	31.49%	29.70%	28.07%	26.56%	25.17%	23.89%
	44.56%	41.29%	38.41%	35.86%	33.56%	31.50%	29.62%	27.92%	26.35%	24.91%	23.57%	22.33%	21.18%	20.11%	19.10%

Table 23: IRR Results from 160 - 300 km for Amine Absorption

Length (km)	160	170	180	190	200	210	220	230	240	250	260	270	280	290	300
IRR (yr-%)	20.08%	18.77%	17.58%	16.48%	15.46%	14.51%	13.63%	12.80%	12.03%	11.30%	10.61%	9.96%	9.35%	8.77%	8.21%
	21.05%	19.72%	18.51%	17.39%	16.35%	15.38%	14.48%	13.63%	12.84%	12.09%	11.39%	10.72%	10.09%	9.49%	8.92%
	22.64%	21.38%	20.23%	19.16%	18.18%	17.26%	16.41%	15.61%	14.87%	14.16%	13.50%	12.88%	12.29%	11.73%	11.19%
	20.82%	19.54%	18.36%	17.27%	16.26%	15.32%	14.44%	13.62%	12.84%	12.11%	11.42%	10.77%	10.15%	9.56%	9.00%
	22.22%	20.91%	19.72%	18.60%	17.57%	16.61%	15.71%	14.86%	14.07%	13.32%	12.61%	11.94%	11.30%	10.70%	10.12%
	22.41%	21.12%	19.94%	18.83%	17.81%	16.85%	15.96%	15.11%	14.32%	13.57%	12.87%	12.20%	11.56%	10.95%	10.38%
	22.26%	21.01%	19.84%	18.76%	17.76%	16.82%	15.93%	15.11%	14.32%	13.59%	12.89%	12.22%	11.59%	10.99%	10.42%
	23.80%	22.53%	21.36%	20.27%	19.25%	18.30%	17.40%	16.55%	15.76%	15.00%	14.29%	13.61%	12.96%	12.34%	11.76%
	23.71%	22.48%	21.34%	20.28%	19.29%	18.35%	17.48%	16.65%	15.86%	15.12%	14.42%	13.75%	13.11%	12.50%	11.92%
	22.69%	21.57%	20.53%	19.55%	18.62%	17.76%	16.93%	16.15%	15.42%	14.71%	14.04%	13.41%	12.80%	12.21%	11.66%
	18.15%	17.26%	16.41%	15.62%	14.86%	14.14%	13.46%	12.81%	12.18%	11.59%	11.02%	10.48%	9.95%	9.45%	8.96%